ChemComm

HIGHLIGHT

View Article Online
View Journal | View Issue

Cite this: *Chem. Commun.*, 2023, **59**, 7302

Recent advances on covalent organic frameworks (COFs) as photocatalysts: different strategies for enhancing hydrogen generation

Chang-Cheng Gu,[a] Feng-Hua Xu,*[b] Wei-Kang Zhu,[a] Run-Juan Wu,[a] Lu Deng,[a] Jun Zou,[a] Bai-Cheng Weng*[b] and Ri-Long Zhu*[a]

Received 22nd April 2023,
Accepted 11th May 2023

DOI: 10.1039/d3cc01970e

rsc.li/chemcomm

The excessive use of traditional fossil fuels has led to energy and environmental pollution problems. Solar-driven hydrogen generation has attracted much attention in recent years owing to its environmental friendliness and economic feasibility. So far, a series of photocatalysts have been advanced. Unfortunately, these photocatalysts face some issues including poor sunlight harvesting ability, weak photo-corrosion resistance, broad band gap, bad stability, inferior hydrogen evolution rate and so on. It just so happens that COFs have emerged to provide an opportunity for settling these issues. Covalent organic frameworks (COFs), a novel family of porous materials with regular porosity and tunable physicochemical structures, have been extensively explored as photocatalysts for hydrogen production. Moreover, their photocatalytic activities are highly structurally dependent. In this review, we mainly focus on the linkage chemistry and disparate strategies for boosting COF-based photocatalytic hydrogen generation performance in detail. The prospects and obstacles confronted in the development of COF-based photocatalysts and proposals to settle dilemmas are also discussed.

1 Introduction

Energy over-exploitation has led to a series of environmental issues, which severely threaten the survival and flourishment of humankind. Therefore, it is urgent to exploit sustainable energy sources.[1–9] Hydrogen, as an eco-friendly and pollution-free energy source, has tremendous potential to solve the current energy problems. At present, there is a need to develop low-cost and outstanding hydrogen production technologies.[10–13]

Photocatalytic water splitting using solar energy for hydrogen evolution, where solar energy is directly converted into chemical energy,[14,15] is becoming one of the most desirable pathways to resolve the issues of overutilization, limited reserves and negative environmental impacts associated with

[a] *Advanced Catalytic Engineering Research Center of the Ministry of Education, Department of Chemistry and Chemical Engineering, Hunan University, Changsha, Hunan Province 410082, China. E-mail: zrlden@hnu.edu.cn*
[b] *Department of Chemistry and Chemical Engineering, Central South University, Changsha, Hunan Province 410083, China. E-mail: xfhuachina@sina.com, bcweng@mail.csu.edu.cn*

Chang-Cheng Gu

Chang-Cheng Gu is currently a PhD candidate at Hunan university. He received his bachelor's degree and master's degree from Nanchang Hangkong University in 2017 and 2020, respectively. His research is mainly aimed at the preparation of covalent organic frameworks and their applications in photoelectric chemistry.

Feng-Hua Xu

Feng-Hua Xu joined Professor Bai-Cheng Weng's group at Central South University as a lecturer after completing her postdoctoral work at the University of Texas-RGV, USA. She received her PhD from Shanghai Institute of Applied Physics, Chinese Academy of Sciences. Her scientific interests include the design and synthesis of nanocomposites and their application in catalysis and biosensing.

fossil fuels. The photocatalytic decomposition of water has the following virtues: (1) it employs two of the most clean and renewable resources that are readily available to us; (2) it is performed at room temperature and pressure, with little restriction on experimental equipment; (3) selective hydrogen and oxygen production without gas separation; (4) the reactant water and products hydrogen and oxygen are clean, with no greenhouse gas emissions, realizing the concept of environmental protection at the source. In the photocatalytic hydrogen evolution reaction (HER), the key is the development of efficient photocatalysts. Over the last few decades, plenty of semiconductor nanostructures and nanocomposites, such as metal oxides,[16–18] metal sulfides,[19–21] metal nitrides,[22–24] graphitic carbon nitrides (g-C_3N_4)[25–27] and metalorganic frameworks (MOFs),[28–32] have been extensively investigated as photosensitizers for H_2 generation. Unfortunately, these photocatalysts have many shortcomings, such as a narrow light response range, weak photo-corrosion resistance, broad band gap and inferior HER rate, which hinder their practical process in photocatalytic hydrogen generation.

Accordingly, huge efforts have been made to develop new and more efficient photocatalysts. Covalent organic frameworks (COFs), a family of crystalline porous polymers, are constructed from light elements (C, H, O, B, N, *etc.*) *via* reversible reactions to form stable and strong covalent bonds that are extended at 2D or 3D interfaces with in-plane π-conjugated and reticulated structures.[33,34] In 2005, since the first COF was reported by Yaghi,[35] the research of COFs has elicited a dramatic response from researchers and has gained traction. The unique topology of COFs endows them with excellent adsorption capacity, enormous specific surface area, adjustable porosity, and long-range orderliness and recyclability, resulting in their tremendous superiority in applications involving photocatalytic water splitting, drug delivery, adsorbing and separating gas, sensors, energy storage, and heterogeneous catalysis.[36–40]

COFs are very suitable photocatalysts for photocatalytic hydrogen production. COFs have designable structures and layered stacking arrays, resulting in narrow band gap and solar-harvesting ability. And the extended π-conjugation within 2D or 3D frameworks facilitates electron transfer and transport. In addition, COFs with high specific surface areas and porous structures can easily chelate metal co-catalysts to enhance photocatalytic activity. Moreover, the covalent linkages present in COFs lead to their insolubility in the solvents, as well as their stability under photocatalytic conditions, meaning that they can be recycled.[41–47] In this review, we give an overview of the research advancement of COFs as photosensitizers for photocatalytic hydrogen evolution through a comprehensive literature survey. Subsequently, the advantages and reasons for the diverse types of linkages for H_2 photoproduction are discussed in detail. Afterwards, a series of strategies are described to enhance light harvesting capability, suppress electron–hole recombination and accelerate carrier migration speed for boosting photocatalytic hydrogen generation performance from the perspective of structural engineering, linkage predesign, band gap engineering, crystallinity optimization, metal species utilization and COF-based hybrids.

2 Linkage chemistry

The formation of COFs is based on polycondensation reactions between building monomers, where covalent bonds confer structural scalability and specific functional roles to COFs, and further influence their crystallinity and chemical stability. An in-depth understanding of linkage chemistry is relevant to the rational design of high-performance COF-based photocatalysts. In this section, we give an overview of widely used covalent linkages, covering boronic esters, imines, hydrazones, vinylenes, triazine linkages and so on (Fig. 1).

2.1 Boronic ester linkages

The first COF was synthesized by Yaghi using a simple one-step condensation reaction between phenyl diboronic acid and hexahydroxytriphenylene.[35] Despite the high reversibility of boronic ester linkages endowing COFs with high crystallinity, their structures are easily damaged by hydrolysis during photocatalytic hydrogen precipitation, which limits their application in this field.

2.2 Imine linkages

Imine-based COFs are constructed by the acid-catalysed co-condensation of amine and aldehyde derivatives based on a

Bai-Cheng Weng

Bai-Cheng Weng is currently a professor at Central South University, China. He received his PhD from Shanghai Institute of Microsystem and information technology, Chinese Academy of Sciences, in 2011. His research interests concentrate on discovering and designing new materials for photocatalytic and electrocatalytic water splitting.

Ri-Long Zhu

Ri-Long Zhu is currently a professor at Hunan University, China. He received his PhD from Hunan University in 2009. His research is mainly focused on environmental electrochemistry, environmental pollution prevention and control, environmental monitoring and evaluation, water resources protection and utilization.

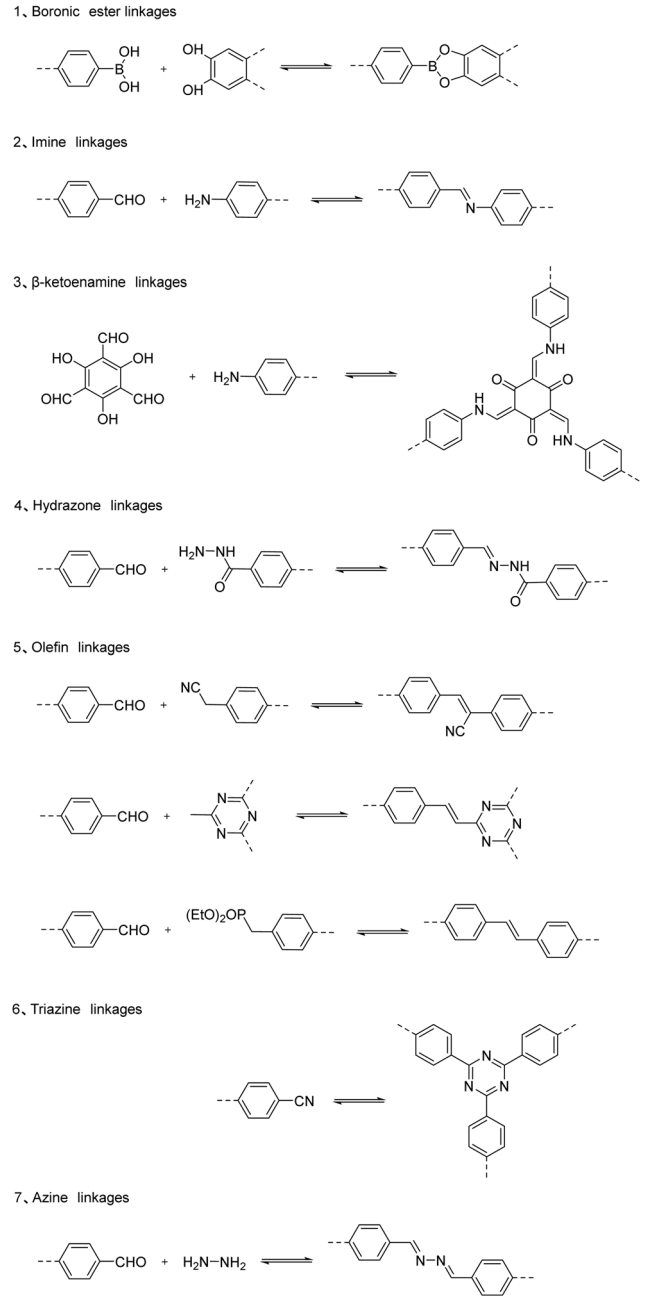

Fig. 1 Linkage chemistry for COF-based photocatalytic hydrogen production.

Schiff-base reaction. Compared with boronic ester linkages, imine-bonded COFs exhibit less reversibility but better stability, making them the most frequently used for photocatalytic HER. The synthesis of imine-based COFs involves two processes. Firstly, building units are covalently linked in an ordered and pre-designed manner and amorphous precipitates are formed *via* the acid-catalysed co-condensation of amine and aldehyde derivatives. Then, as the reactions proceed, the reversibility of imine bonds allows the COFs to form self-healing materials, which have the ability to error-check and proofread their structures. The final amorphous precipitates can thus be corrected to COF crystals. The polarizability of carbon–nitrogen bonds leads to the synthesized imine-based COFs exhibiting weak π-electron delocalization and poor stability in strong acids and bases.[48,49] β-Ketoenamine-based COFs, which are derived from imine-linked COFs, show superior stability and HER rate under identical conditions because of keto–enol tautomerism.

2.3 Hydrazone linkages

Hydrazone-based COFs are formed *via* the co-condensation of amine and hydrazide derivatives. Since hydrazone-linked COFs were initially synthesized by Yaghi *et al.*,[50] there has been much research progress based on hydrazone-linked COFs for the HER. These materials are more resistant to hydrolysis and more stable than imine-linked COFs owing to the p-π conjugation effect between nitrogen atoms and C=O bonds. Moreover, the insolubility and difficult synthesis of aromatic hydrazone building blocks has resulted in there being relatively few reports on hydrazone-linked COFs for photocatalytic hydrogen generation.

2.4 Olefin linkages

Since the first sp^2-carbon-linked COF was reported by the Feng group *via* a Knoevenagel polycondensation reaction in 2016,[51] olefin-linked COFs (V-2D-COFs) have attracted extensive attention for their application in the area of photocatalytic hydrogen production, attributed to the advantages of their sturdy and fully π-conjugated backbone structures and high chemical stability under harsh conditions, although the low reversibility of C=C bonds makes the synthesis of V-2D-COFs quite challenging. Currently, the methods to fabricate vinylene-linked COFs mainly include aldol-type polycondensation, Knoevenagel polycondensation and Horner–Wadsworth–Emmons (HWE) polycondensation reactions. It is found that fewer sp^2-COFs have been adopted for visible-light-driven hydrogen generation than imine-based COFs because of their lower crystallinity.

2.5 Triazine linkages and other linkages

Covalent triazine frameworks (CTFs) as a class of amorphous organic polymers are attained *via* the trimerization of aromatic nitriles with excellent conjugation and have already been proven to exhibit outstanding performance in photocatalytic HER. Due to the limited reversibility of the reactions and limited building monomers, CTFs are less crystalline and there is a small number of different types. Other linkages, such as oxadiazoles and azines with limited chemical stability and crystallinity, have also been successfully prepared for the rational design of COF-based photocatalysts.

3 Different design strategies for COF-based photocatalytic hydrogen evolution

In 2014, Lotsch *et al.* synthesized a hydrazone-linked COF *via* a Schiff-base polycondensation reaction and applied it for the first time in photocatalytic hydrogen production (Fig. 2).[52] The amount of hydrogen produced in 5 h reached 1.97 mmol g^{-1} h^{-1}

according to HER experiments. Since then, with the rapid development of COF chemistry, a series of COFs have been established. In this section, we focus on the strategies to enhance photocatalytic hydrogen generation performance that have been reported in recent years.

3.1 Structure engineering

Building unit pre-design is an outstanding advantage of COFs, which offers great possibilities for the rational synthesis of photocatalysts. By selecting and modifying building blocks, the photochemical properties of COFs can be regulated at the molecular level. Moreover, the pre-designed structures of COFs allow post synthetic modifications to achieve new performance and structural optimization. Careful structure engineering offers a platform to explore structure–property–activity relationships for efficient photocatalytic H_2 evolution, including D–A interaction, functional group modified building blocks, π-conjugation degree, defect engineering, post-modification and isomer design (Table 1).

3.1.1 Donor–acceptor interaction. Donor–acceptor (D–A) molecules are a family of functional compounds consisting of electron donors and acceptors. Integrating D–A moieties is a valid strategy by which to facilitate the electron–hole separation and charge transport of COFs. Adopting this strategy, a variety of COFs have been prepared.[53–68] For example, Yang *et al.* designed PETZ-COF *via* the solvothermal reaction of electron-donating 4PE-4NH_2 and electron-deficient TZTZ-2BA for photocatalytic H_2 generation. As a comparison, a COF (PEBP-COF) without D–A moieties was also constructed using 4PE-4NH_2 to react with BP-2BA (Fig. 3A).[53] The results exhibited an excellent hydrogen evolution rate (7324.3 μmol g^{-1} h^{-1}) of PETZ-COF with the assistance of Pt as a co-catalyst and ascorbic acid as a sacrificial reagent, which was an order of magnitude greater than that of PEBP-COF. Under optimal conditions, the longstanding hydrogen evolution experiment showed good stability (Fig. 3B). Wen *et al.* adopted TzDA and PyTA as building blocks to establish a new D–A system PyTz-COF (Fig. 4A).[54] The photocurrent reached 100 mA cm^2 at 0.2 V and a hydrogen production rate of 2072.4 μmol g^{-1} h^{-1} was exhibited by PyTz-COF. From Fig. 4B, the amount of hydrogen production increased quickly in the first hour, increased moderately in the second hour, and reached a peak in the fourth hour.

Vinylene-based COFs are attractive photocatalysts because of their fully π-conjugated skeletons that promote carrier migration. The highly ordered D–A conjugation system in olefin-linked COFs is beneficial to photocatalytic HER activity. Zhao *et al.* fabricated three new sp^2-carbon-linked COFs (BTH-1,2,3) using benzobisthiazoles moieties as electron-deficient receptors.[55] The high crystallinity of these three COFs was achieved using a neutral $AcONH_4$-catalyzed condensation to improve the reversibility of the Knoevenagel polycondensation reaction. The authors also explored the effect of other base catalysis on crystallinity, using DBU, Cs_2CO_3, and NaOH. Unfortunately, no indication of crystallinity was observed using these bases. Owing to D–A interactions between two organic monomers, the carrier migration and transport capabilities of BTH-3 were improved, which delivered the best photocatalytic HER performance of 15.1 mmol g^{-1} h^{-1} under visible light illumination, far better than those of BTH-1 (10.5 mmol g^{-1} h^{-1}) and BTH-2 (1.2 mmol g^{-1} h^{-1}). Chen and co-workers prepared three D–A type COFs to explore the influence of weak donors on photocatalytic HER ability by varying donor monomers from phenyl to 2,5-dimethylbenzene and 3,3′-dimethyl-1,1′-biphenyl in the skeletons.[56] The results revealed that the D–A interaction was enhanced with an increase in the donor conjugation effect, with TM-DMA-COF exhibiting the best HER rate of up to 4300 μmol g^{-1} h^{-1}.

Adjusting the space length between the receptor units of COFs to match carrier diffusion extent is the way to develop novel COF platforms to advance energy/electron transfer and exciton separation for hydrogen production. Chen *et al.* adopted this method, selecting 2,2′-bipyridine (Bpy) and 1,3,5-triazine (TA) acceptor units for engineering three olefin-

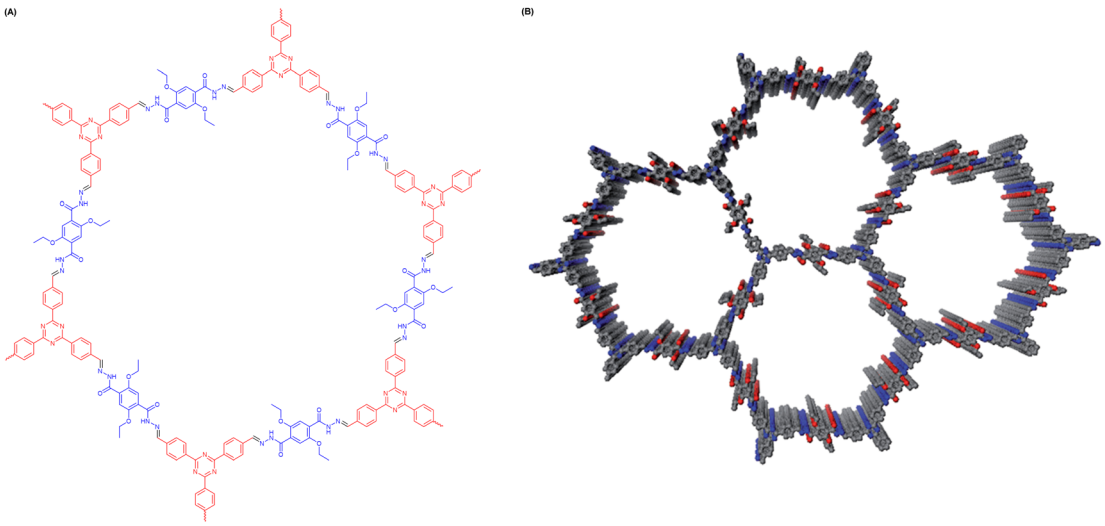

Fig. 2 (A) Chemical structure of TFPT-COF. (B) A hexagonal lattice of TFPT-COF. Reprinted with permission, copyright, 2014, Royal Society of Chemistry.[52]

Table 1 Some of the COF-based photocatalysts for hydrogen evolution synthesized *via* the structure engineering method in Section 3.1

COF-based photocatalysts	Light irradiation	HER (μmol g^{-1} h^{-1})	AQE (%)	Ref.
PETZ-COF	>420 nm	7324.3	3.64 (520 nm)	53
BTH-3	>420 nm	15 100	1.256 (500 nm)	55
BTH-2	>420 nm	1200	0.241 (500 nm)	55
BTH-1	>420 nm	10 500	1.925 (500 nm)	55
NKCOF-108	>420 nm	11 600	2.96 (520 nm)	58
NKCOF-113-M	>420 nm	13 100	56.2 (475 nm)	59
BDF-TAPT-COF	AM 1.5	1390	7.8 (420 nm)	63
BT-TAPT-COF	≥420 nm	949	0.19 (410 nm)	65
CYANO-CON	>420 nm	134 200	82.6 (450 nm)	69
Py-ClTP-BT-COF	>420 nm	8875	8.65 (420 nm)	70
Tp-PDA	>420 nm	600	0.76 (420 nm)	72
Tp-DBN	>420 nm	1800	2.12 (420 nm)	72
TZ-COF-4	>420 nm	4296	1.3 (420 nm)	77
FOO-COF	>420 nm	119.1	20.5 (435 nm)	80
USTB-10	≥420 nm	21 800	0.68 (420 nm)	81
sp^2c-COF_{ERDN}	≥420 nm	2120	0.48 (495 nm)	83
PyTA-BC	≥420 nm	5030	1.46 (420 nm)	85
PyTA-BC-Ph	≥420 nm	2763	1.83 (420 nm)	85
COF-BPDA	>420 nm	3230	2.1 (435 nm)	87
COF-DFB	>420 nm	2100	0.7 (435 nm)	87
g-$C_{40}N_3$-COF	>420 nm	4120	4.84 (420 nm)	88
TAPT-COF-7	>420 nm	33 910	14.43 (520 nm)	89
Tp-2C/BPy^{2+}-COF (19.10%)	>420 nm	34 600	6.93 (420 nm)	90
ODA-COF	≥420 nm	2615	0.42 (420 nm)	91
TtaTfa	>420 nm	20 700	1.43 (450 nm)	92
v-2D-COF-NO1	>400 nm	1970	—	94

linked COFs *via* melt polycondensation in the presence of benzoic anhydride as a catalyst.[59] As a consequence, the best HER performance of 13.1 mmol g^{-1} h^{-1} was exhibited by NKCOF-113-M, whose space length between Bpy and TA elements was moderated (Fig. 5). Also, NKCOF-113-M attained an apparent quantum yield of 56.2% at 475 nm, the second highest value compared to previously reported COF-based photocatalysts, only lower than that of CYANO-CON.[69] These experimental results could be explained by the longer excited state lifespan and higher photocurrent of NK-COF-113-M.

3.1.2 Functional group modified building blocks. Immobilizing functional groups on the backbones of building units enables the modulation of electron push–pull effect and narrowing of the band gap, thus facilitating the separation and transfer of photoinduced excitons. Hence, strong electron-absorbing groups (like halogen atoms, heteroatomic atoms) and electron-donating groups (like methyl, methoxy) are often adopted to modify COF structures to boost photocatalytic HER.[69–80]

Halogen atoms as typical electron-absorbing groups exhibit good electronegativity, which can regulate the localized electron cloud density and delocalization of conjugated building blocks and promote the separation transfer of electrons to enhance HER ability. Chen *et al.* selected a benzothiadiazole (BT) acceptor as a qualifiable building block to fabricate Py-XTP-BT-COFs (X = H, F, Cl) *via* chlorination and fluorination (Fig. 6).[70] The existence of F and Cl atoms not only improves the charge separation efficiency between the skeletons, but also reduces the activation energy of H_2 generation, resulting in Py-ClTP-BT-COF and Py-FTP-BT-COF revealed exciting HER rates of 8875 μmol g^{-1} h^{-1} and 2875 μmol g^{-1} h^{-1}, higher than that of pristine Py-HTP-BT-COF. Moreover, Py-ClTP-BT-COF exhibited an apparent quantum efficiency (AQE) of 8.65% at 420 nm, which is one of the highest values reported in COF photocatalysis.

Aside from halogen atoms, as a typical electron-absorbing group, the presence of the cyano group on the backbone of the building units also improves the separation and transfer of photogenerated carriers and effectively reduces the energy barrier for H_2 generation. For instance, Yang *et al.* incorporated an appropriate D–A (β-ketene-cyano) pair into a COF nanosheet (CYANO-CON) (Fig. 7A), which significantly prolonged the charge carrier lifetime, resulting in a record-breaking AQE of 82.6% at 450 nm for hydrogen evolution and the topmost HER activity of 2684 μmol h^{-1} (Fig. 7B).[69] Likewise, Chen *et al.* obtained a cyano-functionalized COF (Tp-DBN) and a pristine COF (Tp-PDA).[72]

Compared to Tp-PDA, the cyano conjugation Tp-DBN induced a stable photocatalytic H_2 evolution performance of

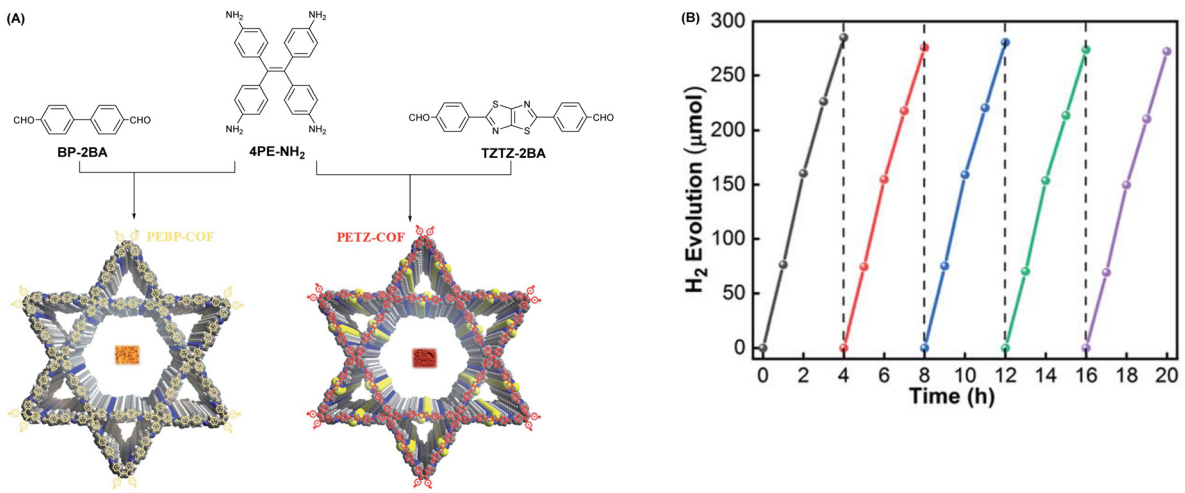

Fig. 3 (A) Schematic description showing the fabrication of PEBP-COF and PETZ-COF. (B) Testing the cycling stability of PETZ-COF hydrogen precipitation for more than 20 h. Reprinted with permission, copyright, 2022, Royal Society of Chemistry.[53]

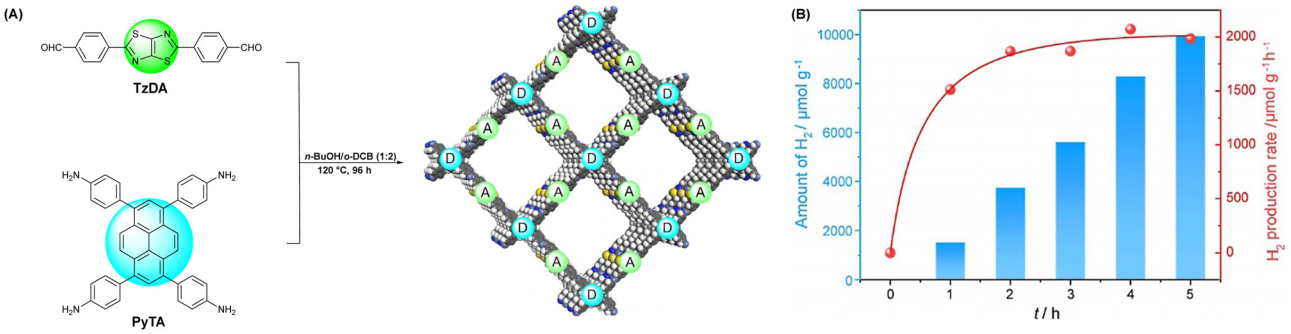

Fig. 4 (A) Schematic diagram of the fabrication of PyTz-COF. (B) Amount and rate of the hydrogen production of PyTz-COF. Reprinted with permission, copyright, 2021, Wiley-VCH.[54]

1.80 mmol g^{-1} h^{-1}. Furthermore, Lotsch and co-workers synthesized four water and photostable 2D N_x-COFs (X = 0, 1, 2 or 3) from hydrazine and triphenylarene aldehydes by doping them with different quantities of nitrogen atoms.[71] With an increase in the nitrogen atom content in the skeleton, the energy band narrows and the valence band becomes smaller, increasing the efficiency of exciton separation. Correspondingly, the hydrogen precipitation capacity was gradually boosted and the N_3-COF showed the best HER rate and AQE.

Different from electron acceptors, electron-donating groups can reinforce the electron delocalization of COFs skeletons. In order to investigate the impact of different substituents and backbones on the H_2 production capability of COFs, the Sun group successfully attached three different groups (H, -$(CH_3)_2$, -NO_2) to the backbone of a β-ketoenamine-based COF (TpPa-COF).[73] The authors systematically investigated the differences between these three COFs in terms of morphology, electron transport and band gap, with the results showing that TpPa-COF-$(CH_3)_2$ exhibited the best hydrogen evolution effect, attributed to the methyl group in TpPa-COF-$(CH_3)_2$ having the most outstanding electron-donating ability.

3.1.3 π-Conjugation degree. A longer π-conjugation can improve light absorption capacity and narrow the π–π* transition of the band gap. This not only increases the photogenerated electron cloud density, but also enhances the proton reduction ability. Hence, adjusting the π-conjugation degree of building blocks is a valid method by which to influence the photocatalytic performance.[81–87]

Jiang *et al.* presented four COFs (USTB-7, USTB-8, USTB-9 and USTB-10) with varying bandgaps (Fig. 8).[81] In contrast to USTB-7 and USTB-8, large conjugation groups conferred USTB-9 and USTB-10 with smaller band gaps. In particular, the 2D dual porous framework of USTB-10 had the biggest pore size and minimum band gap, which brought about the most remarkable hydrogen production ability of 21.80 mmol g^{-1} h^{-1} within a 5 h period. Two π-conjugated photoactive molecular chromophore building blocks, BT and NT, were assembled for band gap engineering. USTB-7 and USTB-8 with the BT chromophore demonstrated a wide absorption peak before 450 nm and a tail peak at ≈550 nm. USTB-9 and USTB-10 with the NT chromophore showed a 100 nm red shift, resulting in smaller band gaps. A reduction in band gap could help to increase the

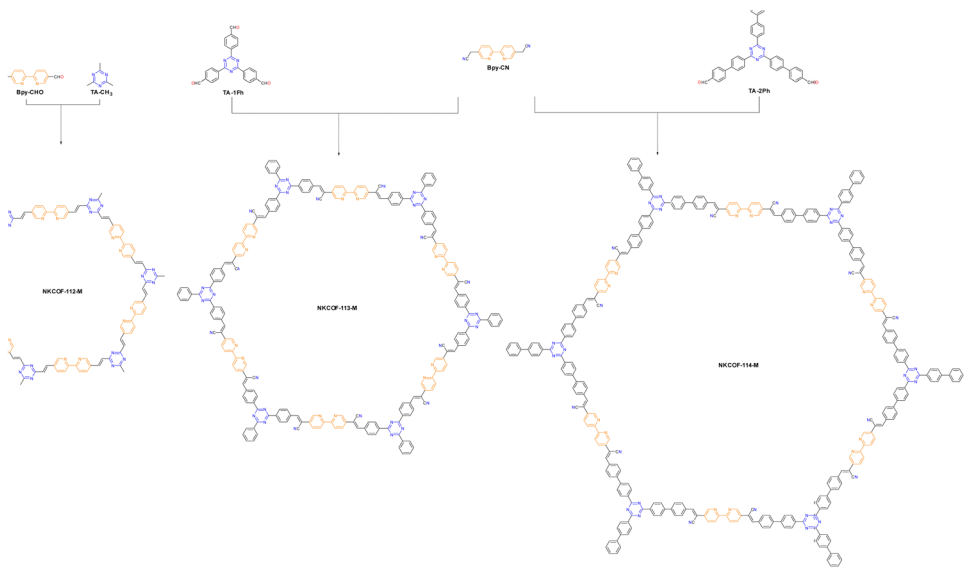

Fig. 5 Synthesis routes and chemical structures of NKCOF-112-M, NKCOF-113-M and NKCOF-114-M.[59]

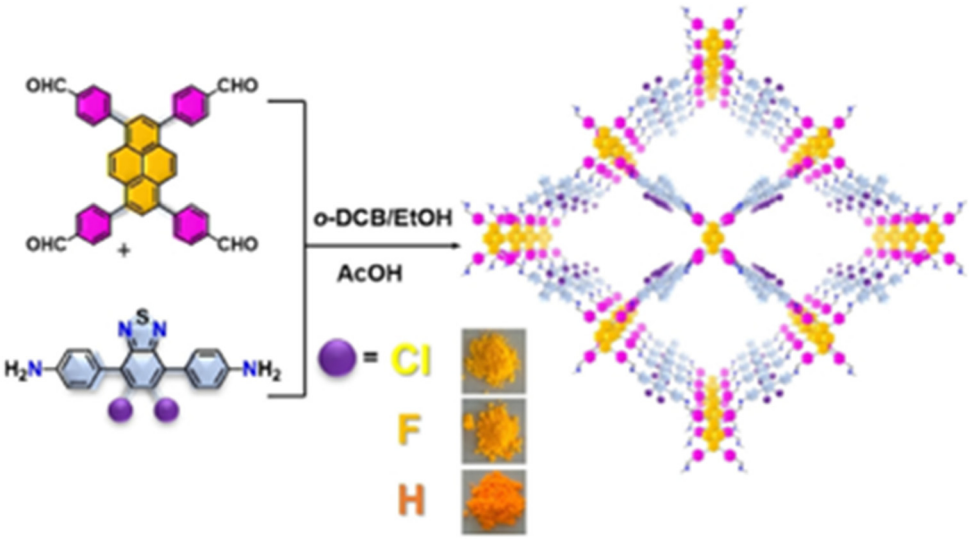

Fig. 6 Synthesis route and chemical structure of Py-XTP-BT-COF. Reprinted with permission, copyright, 2020, Wiley-VCH.[70]

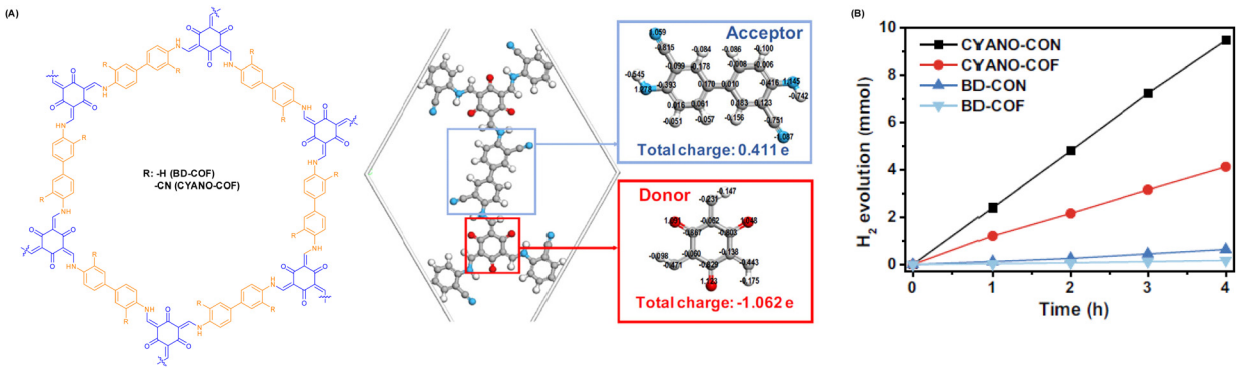

Fig. 7 (A) Structure diagram and charge distribution of CYANO-COF. (B) Time course of the photocatalytic H_2 evolution performance of different COFs and CONs. Reprinted with permission, copyright, 2022, Nature Publishing Group.[69]

range of visible light to promote charge-carrier separation efficiency. Benefiting from this, USTB-9 and USTB-10 attained superior photocatalytic activity compared with USTB-7 and USTB-8.

Zhang *et al.* prepared two COFs, denoted COF-DFB and COF-BPDA, with two similar building blocks *via* an aldol-type polycondensation reaction.[87] The HER experiment confirmed that COF-BPDA exhibited a hydrogen generation rate of 3.23 mmol g^{-1} h^{-1}, almost 1.54 times greater than that of COF-DFB (2.1 mmol g^{-1} h^{-1}), due to the distinctly longer conjugation length of COF-BPDA. Compared to COF-DFB, the conjugated portion of the pyridine ring connected at an adjacent or para position with a longer π-conjugation length endowed COF-BPDA with longer wavelength absorption to improve photocatalytic ability. Additionally, the same team further fabricated three COFs (g-$C_{40}N_3$-COF, g-$C_{31}N_3$-COF, and g-$C_{37}N_3$-COF) with varying conjugation length from the same mesitylene-type monomer with three different aldehydes that possessed similar skeletons.[88] These COFs revealed both hydrogen and oxygen evolution capabilities. Because of excellent light-harvesting characteristics, more electron–hole pairs were produced, which made the optimal HER capability of g-$C_{40}N_3$-COF reach a rate of 4.12 mmol g^{-1} h^{-1} with the help of a Pt co-catalyst, while the OER rate of g-$C_{40}N_3$-COF reached 50 μmol g^{-1} h^{-1} when using 3 wt% Co^{2+} as the co-catalyst, $AgNO_3$ as the electron receptor and La_2O_3 as the pH buffer under visible-light illumination.

3.1.4 Defect engineering. Defect engineering can essentially regulate the coordination condition of active sites and optimize electronic structures to enhance catalytic properties. Defect engineering strategies involve intrinsic defects (atomic vacancies and active edges) and extrinsic defects (metal doping, non-metal doping and hybrid doping). Intrinsic defects are caused by incomplete structures of crystals themselves, while extrinsic defects are caused by the doping of heteroatoms into COFs. To date, tuning the hydrogen generation performance of COF-based photocatalysts *via* a defect engineering strategy has never been reported.

Li *et al.* fabricated TAPT-COF-X with different defect ratios by adding a small amount of regulator to adjust charges and

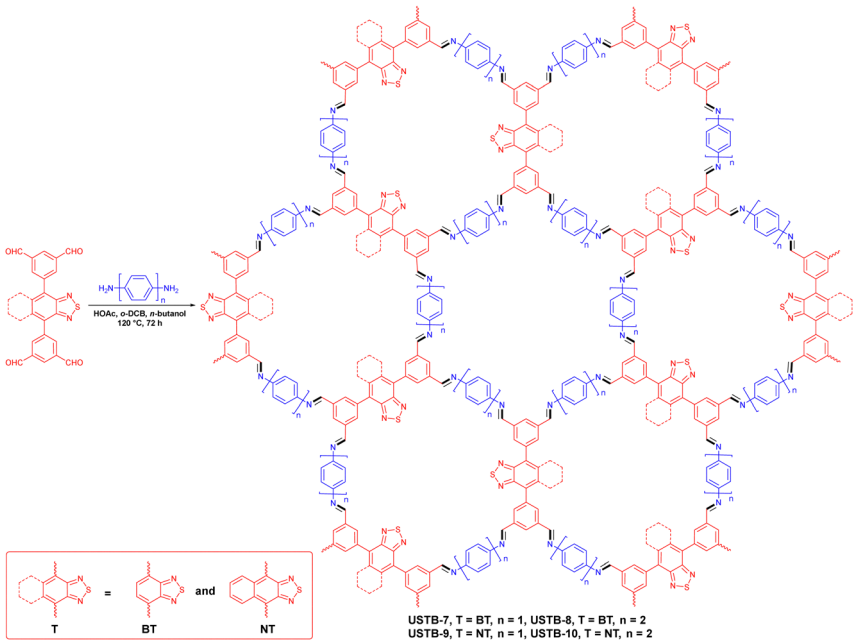

Fig. 8 Schematic diagram for synthesizing USBT-7 to USTB-10.[81]

band structures and generate active sites to promote photocatalytic hydrogen evolution.[89] TAPT-COF-7 exhibited outstanding photocatalytic capability, with a H_2 generation performance of 33.91 mmol g^{-1} h^{-1} in the presence of 3 wt% platinum as the co-catalyst and triethanolamine (TEOA) as the sacrificial agent, due to its minimum conduction band minimum (CBM) potential, which is the closest to the theoretical potential value for hydrogen generation (Fig. 9). On the one hand, TAPT-COF-7 attained the lowest impedance value, which indicated that structural defects enhanced the transfer of electrons. On the other hand, the medium defect level gave the longest lifetime of photogenerated electron-hole pairs for TAPT-COF-7, resulting in higher charge separation efficiency and decreased recombination of photogenerated electrons–holes. These results evidenced that an optimal percentage of structural defects could be introduced into COFs to improve catalytic performance.

3.1.5 Post-modification. Post-modification refers to synthesized COFs being altered *via* post-reaction or functionalization, by attaching different functional groups to their pore surface, while maintaining their structural integrity and properties. Post-modification has been shown to be an effective approach for improving the physicochemical properties of COFs.[90–93]

Electron transfer is a decisive step in the photocatalytic decomposition of water. The layer-by-layer stacked structures of COFs allow active sites to be deeply encapsulated and severely restrict electrons transfer. There are several methods used to enhance COF electron transfer ability: (1) extension of electron delocalization through the design of building blocks and stacked framework structures; (2) modifying substituents and giving alternate connections to acceptor units to regulate the electron push–pull effect; (3) enhancing the separation and transfer of photogenerated electrons and holes by compounding inorganic semiconductors, metal complexes or functional polymers. The electron transfer medium (ETM) can maintain stable electron transfer in the dynamic equilibrium of a chemical reaction, thus improving reaction efficiency. Viologen and its derivatives can act as ETMs with excellent electron donating-accepting ability, where photogenerated electrons can be facilitated to active sites. Guo *et al.* integrated cyclic diquats, which acted as electron-transfer mediators, into a 2,2′-bipyridine-based COF *via* a post-quaternization reaction (Fig. 10).[90] The authors loaded the alkyl chains on two adjacent pyridine nitrogen (from -$(CH_2)_2$- to -$(CH_2)_4$-), quaternized with dibromo alkanes into cyclic diquats, denoted Tp-*n*C/BPy^{2+}-COF (n = 2, 3, 4). In comparison with original COFs, the quaternized Tp-2C/BPy^{2+}-COF demonstrated superior electron-transfer capability, resulting in an outstanding hydrogen evolution activity of 34 600 μmol g^{-1} h^{-1} (involving 19.10 mol% 2C/BPy^{2+}).

Moreover, Wang *et al.* transformed a *N*-acylhydrazone-linked COF (H-COF) into a stable and π-conjugated oxadiazole-linked COF *via* the post-oxidative circularization of a reversible hydrazone linkage to produce an irreversible COF (ODA-COF) (Fig. 11A).[91] After the post-modification of H-COF, the ODA-COF not only maintains its framework crystallinity and porosity, but its chemical stability and π-electron delocalization were also enhanced due to the presence of irreversible bonds, resulting in a superior hydrogen evolution rate of 2615 μmol g^{-1} h^{-1}, which was over four times faster than that of H-COF under the same reaction conditions (Fig. 11B).

3.1.6 Isomer design. It has been found that isomeric monomers can regulate band gap. Zhang *et al.* established two new isomeric benzobisoxazole-based v-2D-COFs (v-2D-COF-NO1 and v-2D-COF-NO2) with two-dimensional layer structures and *trans* and *cis* configurations, respectively, *via* a solid-state Aldol-type polycondensation reaction (Fig. 12A).[94] As illustrated

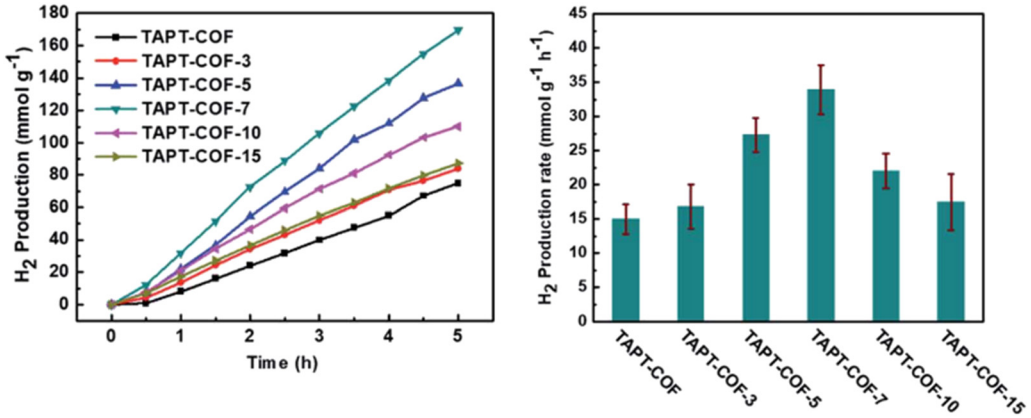

Fig. 9 Time course and HER rate of TAPT-COF-*X*. Reproduced with permission, copyright, 2021, Royal Society of Chemistry.[89]

in Fig. 12B, v-2D-COF-NO1 and v-2D-COF-NO2 achieved conduction band (E_{CB}) values of −3.48 and −4.17 eV, respectively. Compared to the standard potential of H^+/H_2 (−4.44 eV), both E_{CB} values were more negative, which theoretically endowed v-2D-COFs with photocatalytic capability. Although v-2D-COF-NO1 and v-2D-COF-NO2 comprised the same constituent elements and similar apertures, they had different properties. With Pt as the co-catalyst, a hydrogen evolution activity of 1.97 mmol g^{-1} h^{-1} was exhibited by v-2D-COF-NO1, which was more than twice that of v-2D-COF-NO2 (0.86 mmol g^{-1} h^{-1}) (Fig. 12C). This could be ascribed to the smaller band gap and electron effective mass of v-2D-COF-NO1, demonstrating that v-2D-COF-NO1 possessed outstanding π-conjugation, resulting in more opportunities for charge carrier migration in the v-2D-COF-NO1 in-plane conjugate structure. Moreover, charge carrier complexation could be suppressed, thus facilitating the effective separation of electron–hole pairs and the improvement in the photocatalytic hydrogen precipitation performance.

3.2 Linkage pre-design

It is well known that linkage chemistry plays an important role in chemical stability and electronic transfer in COFs. By choosing building blocks with similar skeleton structures as knots, but with different linkages to investigate HER property is necessary (Table 2).[95–97] To this end, Yu and co-authors adopted triphenylbenzene knots and phenyl linkers to explore the effect of three structurally similar COFs with distinct linkages on the photocatalytic hydrogen precipitation performance.[95] The experiments revealed that the HER activity could be tuned with the rate in the order of COF-olefin (2.33 mmol g^{-1} h^{-1}) ≫ COF-imide (<40 μmol g^{-1} h^{-1}) > COF-imine (<40 μmol g^{-1} h^{-1}). Femtosecond transient absorption spectroscopy (Fs-TA) and density functional theory calculations certified that the excellent HER activity of the COF-alkene could be attributed to the cyano-substituted alkene linkages endowing the COF-alkene with strong electron absorption capability in the presence of sacrificial electron donors.

Moreover, the Cai group synthesized three types of COFs (TTI-COF, TTV-COF and TTAN-COF) with identical triphenyltriazine building blocks *via* Schiff-base polycondensation, HWE polycondensation and Knoevenagel polycondensation reactions, respectively (Fig. 13).[96] The group first applied the TTV-COF synthesized *via* the HWE polycondensation reaction to photocatalytic hydrogen generation and researched the

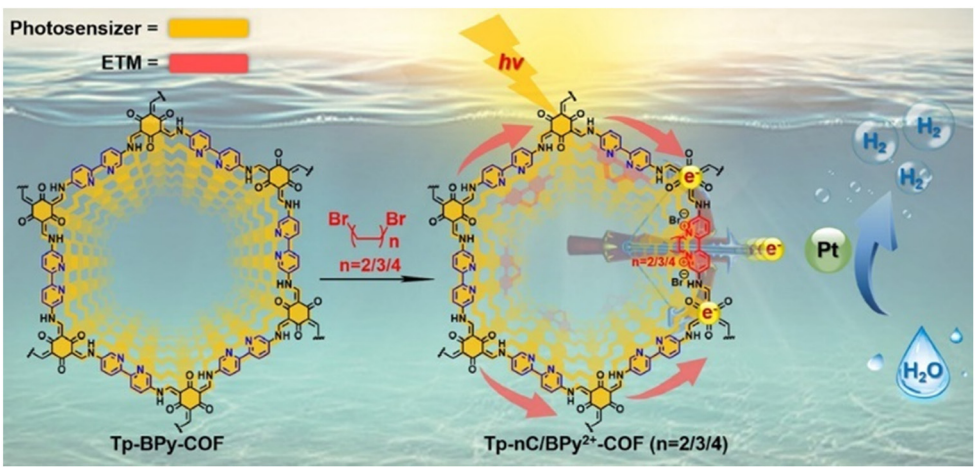

Fig. 10 Synthesis route of Tp-*n*C/BPy^{2+}-COF. Reprinted with permission, copyright, 2021, Wiley-VCH.[90]

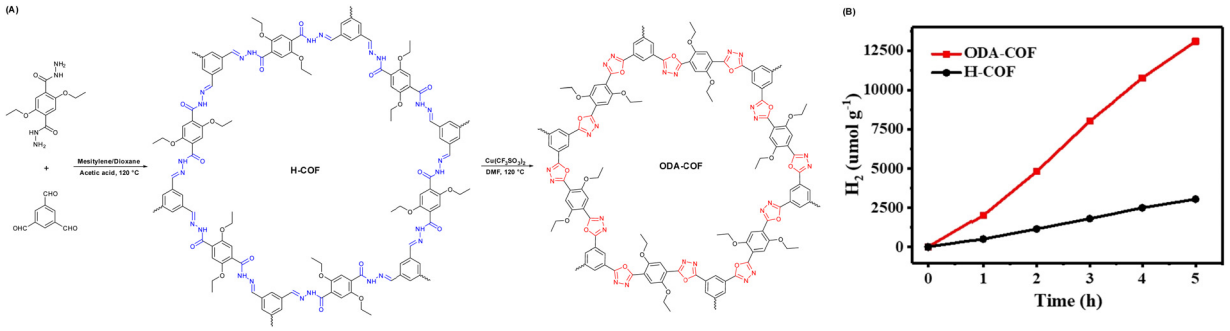

Fig. 11 (A) Synthesis representation and chemical structure of H-COF and ODA-COF. (B) Time course of photocatalytic H_2 evolution capability for H-COF and ODA-COF. Reprinted with permission, copyright, 2022, Wiley-VCH.[91]

influence of different linkages on the HER performance. When Pt was chosen as the co-catalyst and triethanolamine (TEOA) as the sacrificial electron donor (SED), TTV-COF attained a HER activity of 116.58 μmol g^{-1} h^{-1}. Also, a HER activity of 5.50 mmol g^{-1} h^{-1} was achieved with the help of Pt as the co-catalyst and ascorbic acid as the sacrificial electron donor (SED). The reason for the large difference in the results between these two experimental methods was the high oxidation potential of TEOA. Unfortunately, the photocatalytic performance of TTV-COF was not as good as that of TTAN-COF due to the strong electron-absorbing ability of the cyanide group endowing TTAN-COF with admirable chemical stability and light photostability.

3.3 Bandgap engineering

The band gap determines the optical absorption performance of the catalyst, which essentially determines the photocatalytic hydrogen generation reaction ability. To achieve photocatalytic water decomposition, the following two points should be satisfied: (1) the energy of the photons needs to be greater than the band gap value for electrons to jump from the top of the valence band to the bottom of the conduction band; (2) the conduction band bottom of the photocatalysts should be more negative than the reduction potential of H^+/H_2, while its valence band top should be more positive than the oxidation potential of O_2/H_2O.

For photocatalytic hydrogen production, a suitable forbidden band width is extremely important. Firstly, the smaller the band gap, the stronger the light absorption range, but this does not necessarily enhance absorption ability. Secondly, the reduction capacity of electrons and oxidation capacity of holes will be weakened as the band gap becomes smaller, which is not conducive to photocatalytic hydrogen evolution. Finally, the smaller the band gap, the easier it is for electrons to return from the excited state to the ground state. Similarly, the compounding of photogenerated electron–holes increases

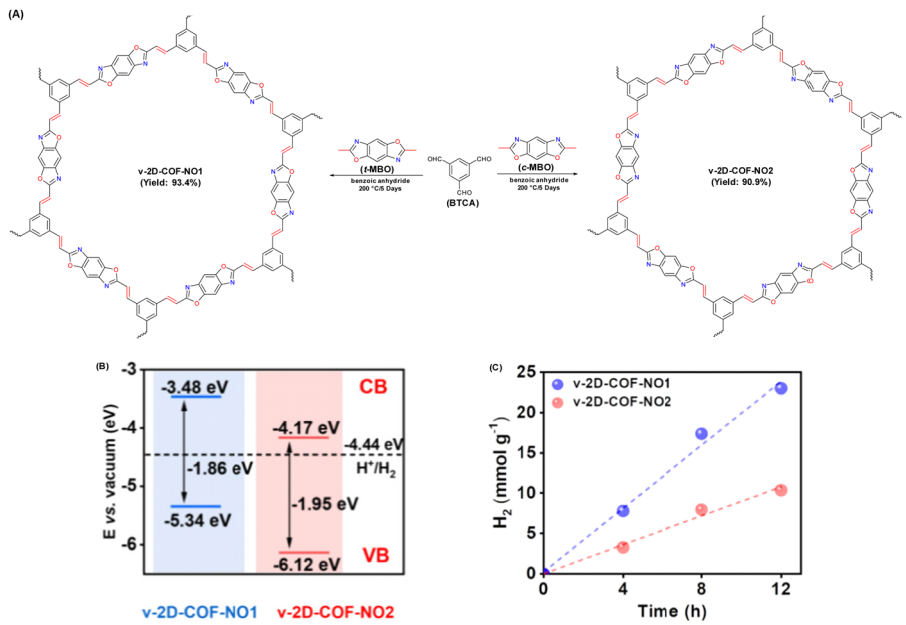

Fig. 12 (A) Schematic illustration for establishing v-2D-COF-NO1 and v-2D-COF-NO2. (B) Energy band position of v-2D-COFNO1 and v-2D-COF-NO2. (C) Time course of photocatalytic H_2 production activity for v-2D-COFNO1 and v-2D-COF-NO2. Reproduced with permission, copyright, 2022, American Chemical Society.[94]

Table 2 Some of the COF-based photocatalysts for hydrogen evolution synthesized *via* the linkage pre-design, bandgap engineering and crystallinity optimization methods in Sections 3.2, 3.3 and 3.4

COF-based photocatalysts	Light irradiation	HER (μmol g^{-1} h^{-1})	AQE (%)	Ref.
COF-alkene	>420 nm	2330	6.7 (420 nm)	95
TTAN-COF	>420 nm	11 940	—	96
PMDA-COF	>420 nm	435.6	—	97
COF-OH-3	≥420 nm	9890	0.15 (420 nm)	98
FL-CTF-2	≥420 nm	1527	11.14	99
COF-JLU100	>420 nm	107 380	5.13 (450 nm)	100
BT-Py_{BuOH}	380–780 nm	11 280	4.88 (420 nm)	101
FS-COF	>420 nm	16 300	3.2 (420 nm)	102

sharply and charge separation efficiency decreases. For the reasons above, COFs with a suitable band gap not only have higher light absorption, but also endow the photogenerated carriers with sufficient redox ability. Thus, it is necessary to regulate the band gap to boost HER photocatalytic performance (Table 2).[98,99] Ning and co-workers discussed COF-OH-*n* (*n* = 0–3, the number of −OH groups) through regulating the number of hydroxyl groups on the backbone of 1,3,5-triformylbenzene to react with 2,4,6-tris(4-aminophenyl)-1,3,5-triazine (TAPT) by tuning the band gaps *via* a proton tautomerization method.[98] When the backbone of 1,3,5-triformylbenzene featured three hydroxyl groups, the produced COF-OH-3 revealed the most suitable band structure of 2.28 eV for hydrogen generation performance and a corresponding HER rate of 9.89 mmol g^{-1} h^{-1}. Fan *et al.* reported an intercalation and exfoliation strategy to establish few-layer CTFs nanosheets when using H_2SO_4 and $(NH_4)_2S_2O_8$ as intercalant and mild oxidant, respectively.[99] The improved HER capability can mainly be ascribed to the narrower band gap of exfoliated CTFs nanosheets compared with that of bulk CTFs, with the AQE of FL-CTF-2 reaching 11.14%.

3.4 Crystallinity optimization

Optimizing the crystallinity of v-2D-COFs is a good way to boost hydrogen generation ability (Table 2).[100–102] When the crystallinity of COFs is higher, their specifications are more ordered and photogenerated electrons are more readily transported.

As shown from Fig. 14A, Liu *et al.* announced that alkene-linked COF-JLU100 could be tuned to have excellent crystallinity and high surface area, as well as outstanding durability and carrier mobility *via* a Cs_2CO_3-catalyzed Knoevenagel condensation reaction combined with a gradient heating strategy.[100] Spectroscopy techniques confirmed that the adoption of the gradient heating method significantly enhanced the crystallinity of the framework compared with the traditional process (120 °C for 72 h). The peaks in the powder X-ray diffraction (PXRD) pattern of COF-JLU100 at 2.71°, 4.69°, 5.42° and 7.17° corresponded to 100, 110, 200 and 210 planes, respectively (Fig. 14C). The broad peak at 25.41° was attributed to the 001 plane and corresponded to an interlayer distance of 3.5 Å (Fig. 14B). As a result, owing to the unprecedented high crystallinity and the presence of a triazine moiety, COF-JLU100 demonstrated a surprising HER activity of 107.38 mmol g^{-1} h^{-1}, exceeding the performance of all previously synthesized COF-based photocatalysts.

During the crystallization of COFs, many factors affect the crystallinity of COFs, with the nature of the solvent being the most influential. Chou *et al.* prepared two types of benzothiadiazole-based COFs with pyrene (Py) and carbazole (Cz) *via* adopting three solvent combinations (mesitylene/1,4-dioxane, *o*-dichlorobenzene/*n*-butanol, and *o*-dichlorobenzene/ethanol),

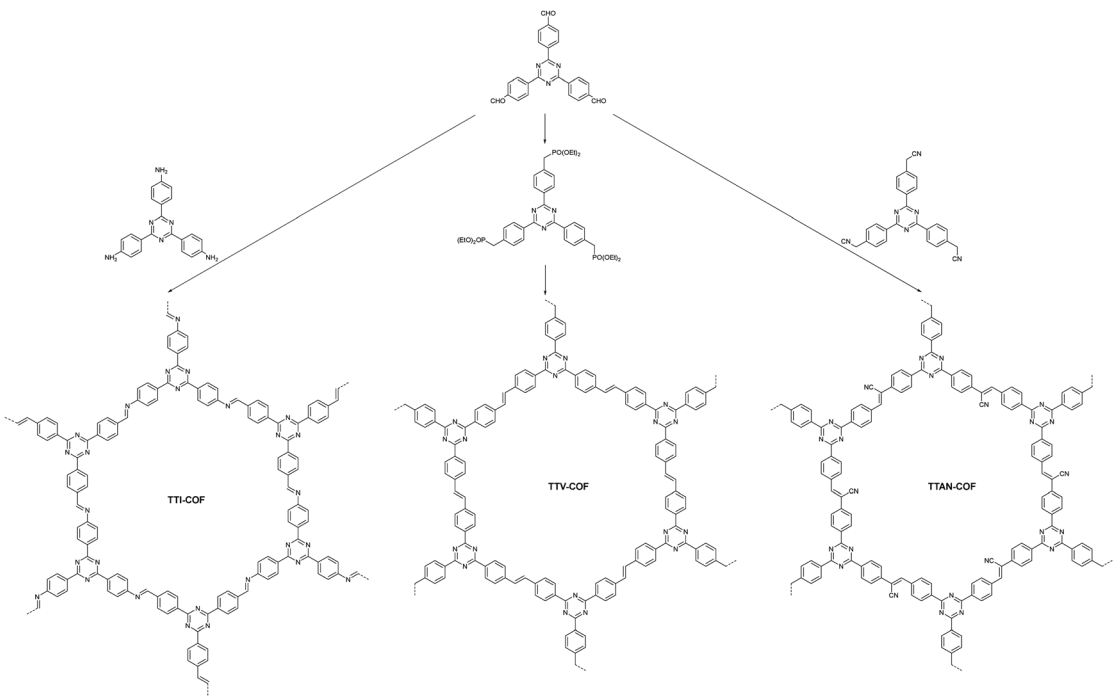

Fig. 13 The synthesis processes of three COFs with different linkages.[96]

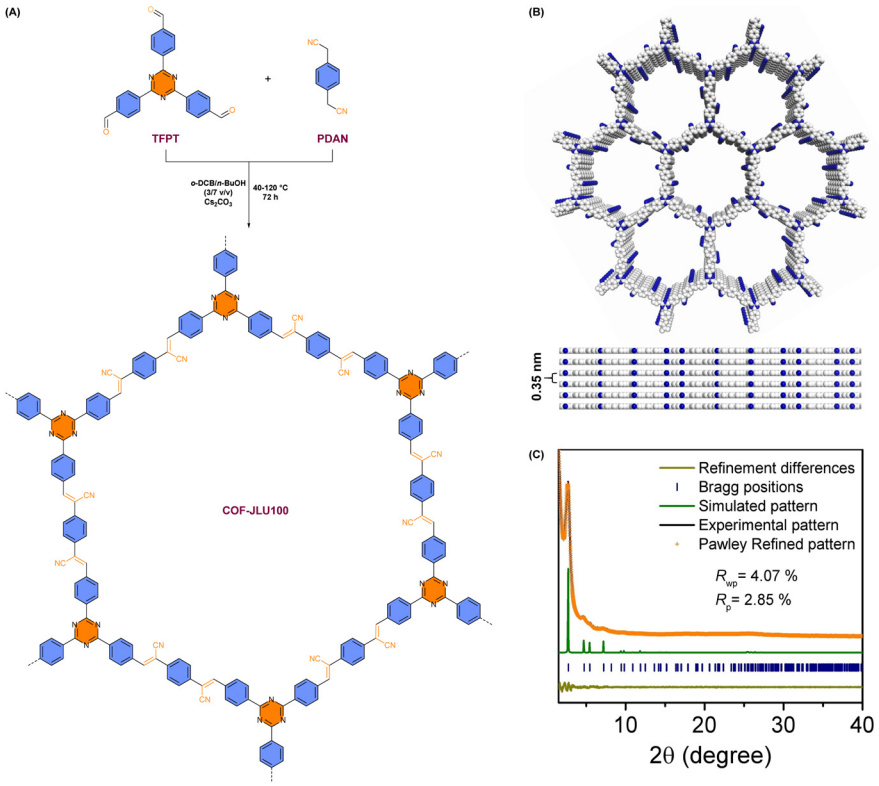

Fig. 14 (A) Schematic diagram for employing COF-JLU100. (B) The eclipsed stacking structure of COF-JLU100 from top and side views. (C) Experimental and simulated PXRD patterns of COF-JLU100. Reprinted with permission, copyright, 2022, Wiley-VCH.[100]

to explore the influence on the crystallinity of COFs and how crystallinity affects the rate of hydrogen precipitation.[101] As a result, with an increase in the solvent polarity, the COFs crystallized more easily. When *n*-butanol and ethanol, two highly polar solvents, were used, the corresponding HER rates also increased.

3.5 Metal species utilization

Conventional metals show poor efficiency in photocatalytic hydrogen evolution, with the disadvantages of being expensive with poor recyclability, whereas COF-based photocatalysts do not face these difficulties. COFs are composed of non-metallic elements, leading to low photogenerated charge efficiency and limited catalytic active sites. On the one hand, COFs with high specific surface areas and high porosities allow them to act as carriers for catalytically active metal nanoparticles. On the other hand, COFs with extensible periodic structures also reduce the aggregation of metal nanoparticles and have a large number of catalytic sites. COFs are linked by covalent bonds and are associated with sluggish kinetic reactions, but usually interact with metal species to exhibit basic proton reduction capability. Therefore, several attempts have been made to enhance the photocatalytic capability by introducing metal active centers into COF skeletons through coordination interactions (Table 3).[103–117]

Based on an aldol-amine condensation reaction between 1,3,5-triformylphloroglucinol (Tp) and 1,4-phenylenediamine (Pa), a series of β-ketoenamine-linked COFs were constructed *via* introducing metal species. Recently, a chiral β-ketoenamine-linked COF was designed and prepared by Guo *et al.*, followed by atomically dispersed Cu(II) being incorporated to form TpPa-Cu(II)-COF.[103] The Cu ions acted as an electron transport medium. When employing L-/D-cysteine as the sacrificial electron donor, the TpPa-Cu(II)-COF generated a flux of H_2 gas of 14.72 mmol g^{-1} h^{-1}, which was comparable to those of abundant chiral COFs employing Pt as the co-catalyst. Moreover, Long and co-workers synthesized two COFs by reacting Tp or 1,3,5-benzenetricarboxaldehyde (BT) with Pa to establish a metal insulator semiconductor (MIS) photosystem *via* electrostatic self-assembly of polyvinylpyrrolidone (PVP) insulator-capped Pt nanoparticles (NPs), where first a charge tunnelling strategy was invented to extract hot π-electrons from photoexcited COF semiconductors for efficient hydrogen evolution.[111] The MIS photosystems showed 32-fold-enhanced carrier efficiency, and a maximal H_2 evolution performance of 8.42 mmol g^{-1} h^{-1} and a turnover frequency of 789.5 h^{-1} were attained.

Nitrogen atoms in bipyridine-based COFs can immobilize various metal ions as catalytic centers to promote HER performance. To this end, three metal 3D COFs, RuCOF-ETTA, RuCOF-TPB and RuCOF-ETTBA, were investigated by Gu *et al.* through integrating the photosensitive Ru(II) tris(2,2′-bipyridine) unit into the COF skeleton (Fig. 15).[104] In the presence of sacrificial ascorbic acid and a Pt co-catalyst, hydrogen evolution rates of up to 6429 μmol g^{-1} h^{-1} for RuCOF-ETTA, up to 14 745 μmol g^{-1} h^{-1} for RuCOF-ETTBA and a maximal hydrogen evolution rate of up to 20 308 μmol g^{-1} h^{-1} for RuCOF-TPB were attained. RuCOF-TPB

Table 3 Some of the COF-based photocatalysts for hydrogen evolution prepared *via* the metal species utilization method in Section 3.5

COF-based photocatalysts	Light irradiation	HER (μmol g^{-1} h^{-1})	AQE (%)	Ref.
TpPa-Cu(II)-COF	>420 nm	14 720	—	103
RuCOF-TPB	>420 nm	20 308	6.95 (420 nm)	104
ZnPor-DETH-COF	>400 nm	413	0.32 (450 nm)	105
Co/Zn-Salen-COF	>420 nm	1378	—	106
Cu-salphen-HDCOF-NSs	>420 nm	36 990	5.77 (420 nm)	107
TpPa-1-SNi-10	>420 nm	10 870	—	108
Ni-COF-SCAU-1	>420 nm	197 460	43.2 (420 nm)	109
$Pd_{0.033}$/TP-TTA/SiO_2	>420 nm	150 000	7.3 (420 nm)	110
Pt-PVP-TP-COF	>420 nm	8420	0.4 (475 nm)	111
Zn-Por-TT COF	>400 nm	8200	—	112
PY-DHBD-COF	>420 nm	42 432	8.4 (420 nm)	113
Py-1P-Ir	460 nm LED light	1358	—	114
Pt_1@TpPa-1	≥420 nm	719	0.38 (420 nm)	115
$Ni(OH)_2$-2.5%/TpPa-2	≥420 nm	1895.99	—	116
N2-COF	AM 1.5	782	0.16 (400 nm)	118
[Co-1b]–COF	AM 1.5	163	—	119

showed excellent properties due to its wide light absorption range, good charge-hole separation efficiency and high hydrophilicity.

Porphyrin molecules possess the advantages of good visible light absorption and high modifiability; their photocatalytic properties can be adjusted by central metal ion coordination. As depicted in Fig. 16A, Wang *et al.* reported four porphyrinic COFs (MPor-DETH-COF, M = H_2, Co, Ni, Zn) by incorporating different transition metals in them employing a Schiff-base polycondensation reaction between porphyrinic aldehydes *p*-MPor-CHO (M = H_2, Co, Ni, Zn) and DETH.[105] As a result, these four hydrazone-linked COFs demonstrated rationally regulated hydrogen photoproduction in the order of CoPor-DETH-COF (25 μmol g^{-1} h^{-1}) < H_2Por-DETH-COF (80 μmol g^{-1} h^{-1}) < NiPor-DETH-COF (211 μmol g^{-1} h^{-1}) < ZnPor-DETH-COF (413 μmol g^{-1} h^{-1}) (Fig. 16B).

In solar-driven water cracking to generate hydrogen, precious metal platinum-based co-catalysts are often employed, making it urgent to find a stable and economical alternative.[118,119] In order to achieve this purpose, Lotsch *et al.* firstly applied chloro(pyridine)cobaloxime as a noble-metal-free molecule co-catalyst to design an azine-linked N_2-COF for photocatalytic hydrogen generation.[118] A hydrogen production rate of 782 μmol g^{-1} h^{-1} was achieved in a mixture of water/acetonitrile. Additionally, the same group constructed another hydrazone-based COF using the same azide-functionalized chloro(pyridine)cobaloxime as a noble-metal-free molecule co-catalyst for photocatalytic hydrogen evolution.[119] During the photoreaction, the interaction between the COF backbone and cobaloxime led to catalyst realignment, which increased the reactivity and prevented the degradation of the catalyst.

3.6 COF-based hybrids

It is well known that the vast majority of COFs have relatively poor electrical conductivity, which easily leads to the recombination of electron–hole pairs. Thus, the introduction of other semiconductors to form COF-based heterojunction hybrids is an effective way to address this drawback (Table 4). The heterogeneous hybrids not only inherit the advantages of each component, but also acquire additional photochemical properties due to the synergistic effect of two components. Moreover, the difference in band gap creates a built-in electric field between two semiconductors, leading to the migration of photogenerated electrons and holes at the interface, where electrons and holes undergo redox reactions in different parts of the heterojunction hybrids. Recently, inorganic semiconductors (MoS_2, CdS, TiO_2, *etc.*) and polymer materials (g-C_3N_4, MOF, *etc.*) have been combined with COFs to advance HER performance.[120–145]

An organic/inorganic direct Z-scheme TpTAP/CdS was designed by Li *et al. via* growing CdS nanosheets *in situ* on a COF surface for photocatalytic hydrogen production (Fig. 17).[120] TpTAP/CdS exhibited the most remarkable HER rate of 47.6 mmol g^{-1} h^{-1} when TpTAP-COF and CdS were combined in a mass ratio of 5 : 4, which was higher than those of pure TpTAP-COF and CdS. Compared with TpTAP/CdS, the authors also explored the HER rate of a heterojunction between TpTAP-COF and 0D particle-like CdS, the results of which revealed that TpTAP/CdS demonstrated better performance. It was observed that the interface between TpTAP-COF and CdS was tightly connected, facilitating the transfer of more photogenerated electrons and reducing the photocorrosion of CdS. Zhang *et al.* established MoS_2/TpPa-1-COF composites by growing TpPa-1-COF *in situ* on an exfoliated MoS_2 dispersion solution.[121] When loaded with 3% wt MoS_2, MoS_2/TpPa-1-COF exhibited a H_2 evolution rate of 5585 μmol g^{-1} h^{-1}, which was 32-fold higher than that of pure TpPa-1-COF.

Black TiO_{2-x} was selected to integrate with TpPa-1-COF to synthesize S-scheme heterojunction hybrids (TiO_{2-x}/TpPa-1-COF) with oxygen defects.[122] Electron paramagnetic resonance (EPR) experiments showed the charge process between TiO_{2-x} and TpPa-1-COF. When TiO_{2-x}/TpPa-1-COF was irradiated with visible light, both TiO_{2-x} and TpPa-1-COF generated electrons and holes on the conduction band (CB) and valence band (VB). Then, the existence of TiO_{2-x} oxygen defects easily trapped electrons on the CB (−0.42 eV), and recombined with holes on the VB (1.37 eV) of TpPa-1-COF. Consequently, more holes were left on the VB (2.83 eV) of TiO_{2-x} to participate in the oxidation reaction, while more electrons were left on the CB (−0.72 eV) of TpPa-1-COF. The H_2 evolution results of TiO_{2-x}/TpPa-1-COF (6 : 4) showed a performance of up to 15.33 mmol g^{-1} h^{-1} and

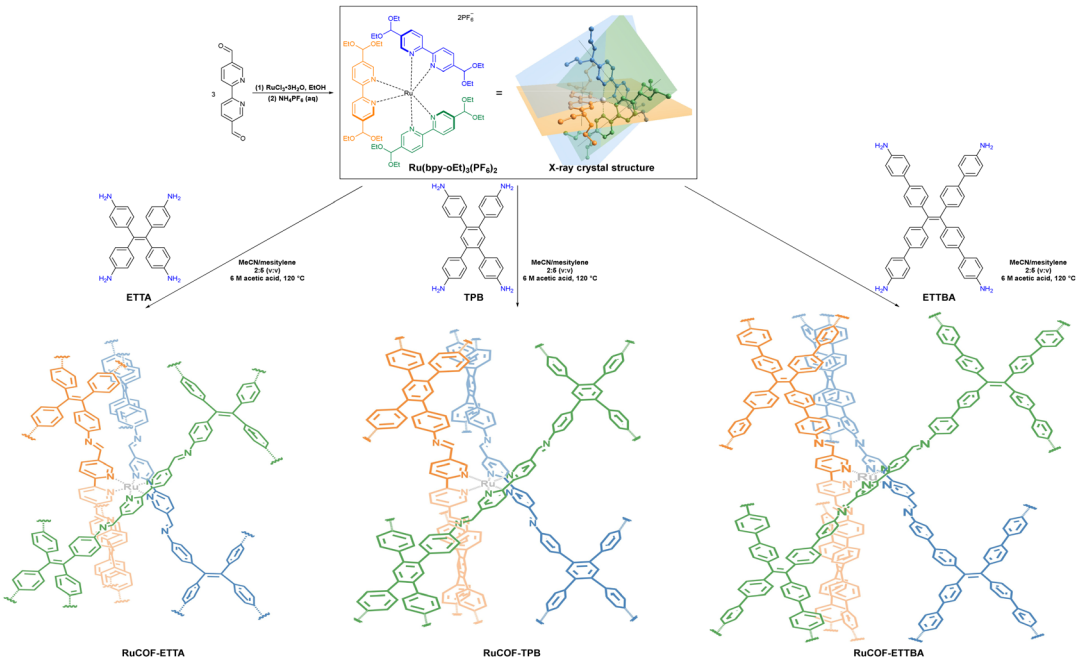

Fig. 15 X-ray crystal structure of $Ru(bpy\text{-}oEt)_3(PF_6)_2$ and synthetic route of Ru-COFs. Adapted with permission, copyright, 2022, Wiley-VCH.[104]

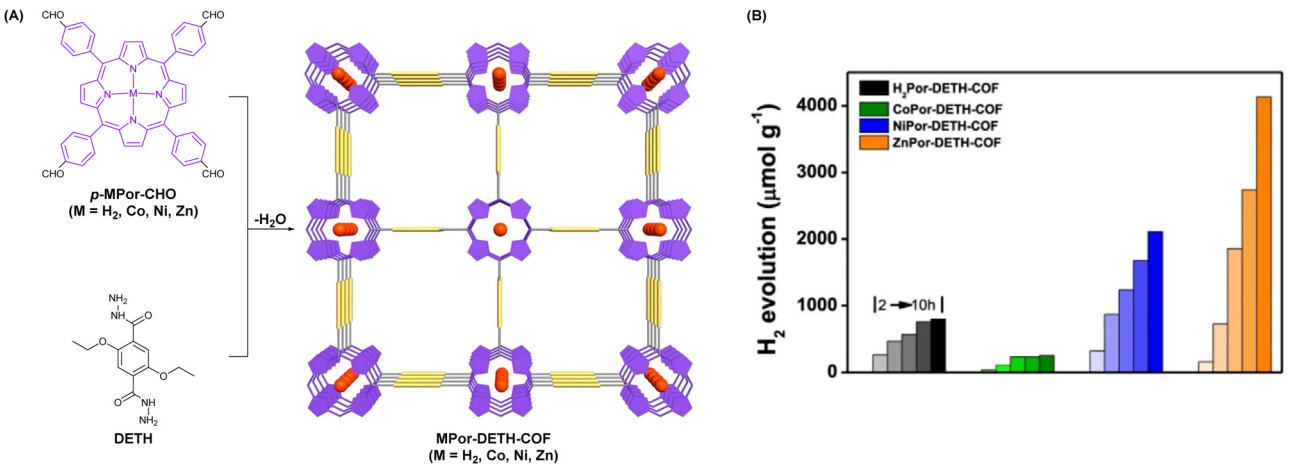

Fig. 16 (A) Schematic illustration for synthesizing MPor-DEPH-COF. (B) Time-dependent photocatalytic H_2 evolution activity of MPor-DEPH-COF. Adapted with permission, copyright, 2021, Nature Publishing Group.[105]

the AQE reached 6.7% at 420 nm. Lan *et al.* fabricated $BiFeO_3$@TpPa-1-COF core–shell Z-scheme heterojunction hybrids *via* covalent bonds by growing TpPa-1-COF on amino-functionalized $BiFeO_3$ nanosheets for overall water splitting (Fig. 18).[123] The carrier separation and utilization efficiency were promoted owing to the synergistic effect of the built-in electric field of the $BiFeO_3$ nanosheets and rich active sites of TpPa-1-COF. $BiFeO_3$@TpPa-1-COF demonstrated HER and OER rates of 1416.4 and 708.2 μmol g^{-1} h^{-1}, respectively.

MOFs, as a class of 2D organic polymers materials, can form 2D/2D heterojunctions with COFs because of their high specific surface area, high porosity and structural modifiability, endowing them with more contact area and a shorter transfer distance, favoring better charge mobility.[124–128] Covalently bonded MOF/COF photocatalytic hydrogen production catalysts were designed and constructed by Lan *et al. via* adopting a one-step method to realize the hybridization of TpPa-1-COF with NH_2-UiO-66 (Fig. 19).[124] The hybrid material inherited the excellent visible light absorption ability of TpPa-1-COF. The covalent bonding between TpPa-1-COF and NH_2-UiO-66 made the composite material stronger and facilitated the transfer of photogenerated electrons through the heterojunction interface. NH_2-UiO-66/TpPa-1-COF (4 : 6), with an exciting HER rate of 23.41 mmol g^{-1} h^{-1}, was found, which was approximately 20 times greater than that of TpPa-1-COF alone. Likewise, Ma *et al.* also used a covalent linkage strategy to synthesize a series of Ti-MOF/COF hybrid materials with

Table 4 Some of the COF-based photocatalysts for hydrogen evolution synthesized *via* the COF-based hybrids methods in Section 3.6

COF-based photocatalysts	Light irradiation	HER (μmol g^{-1} h^{-1})	AQE (%)	Ref.
TpTAP/CdS	>420 nm	47 600	25.23 (420 nm)	120
MoS_2/TpPa-1-COF	>420 nm	5585	0.76 (420 nm)	121
TiO_{2-x}/TpPa-1-COF	≥420 nm	15 330	6.7 (420 nm)	122
$BiFeO_3$@TpPa-1-COF	≥420 nm	1416.4	0.77 (420 nm)	123
NH_2-UiO-66/TpPa-1-COF	>420 nm	23 410	—	124
PdTCPP⊂PCN-415(NH_2)/TpPa	>400 nm	13 980	5.9 (515 nm)	125
MOF-808@TpPa-1-COF	>420 nm	11 880	10.23 (450 nm)	126
30%PEG@BT-COF	>420 nm	11 140	11.2 (420 nm)	129
$Ni_{12}P_5$/TpPa-1-COF	>420 nm	3160	—	134
ATNT-4	>420 nm	14 228.1	9.75 (500 nm)	135
Cu_2O/PyTTA-TPA	>420 nm	12 500	21.5 (450 nm)	140
$[Mo_3S_{13}]^{2-}$@ZnP-Pz-PEO-COF	>420 nm	11 000	5.7 (500 nm)	143
Mo_3S_{13}@EB-COF	>420 nm	13 215	4.49 (475 nm)	145

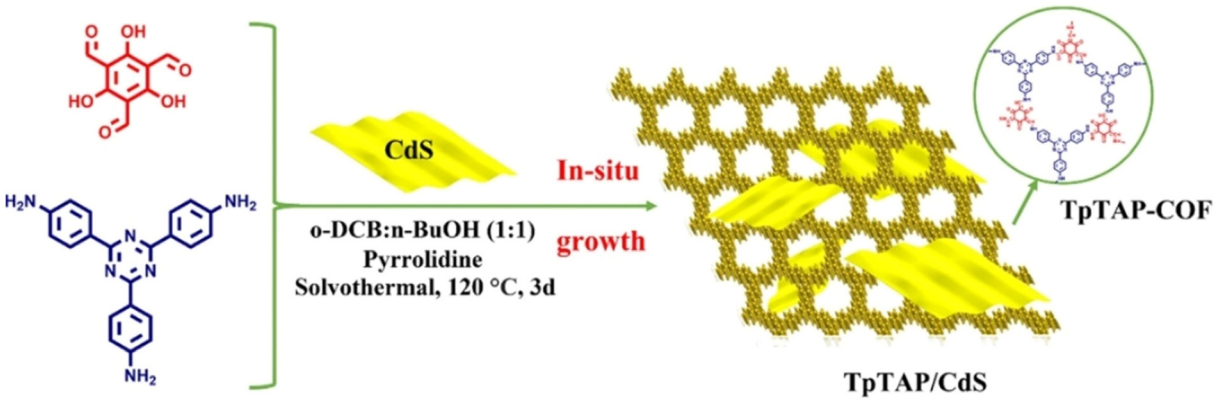

Fig. 17 Schematic illustration for constructing direct Z-scheme TpTAP/CdS. Adapted with permission, copyright, 2023, Elsevier.[120]

outstanding visible light response, appropriate band gap and efficient charge separation for photocatalytic H_2 evolution.[125] During the photocatalytic process, after PdTCPP⊂PCN-415(NH_2) captured light, the photoexcited electrons were transferred to $[Ti_8Zr_2O_{12}(COO)_{16}]$ clusters by means of ligand-to-metal charge transfer. Then, the LUMO of TpPa obtained the photoexcited electrons *via* a covalent junction and further transfered to the Pt NP surface, reducing H^+ to hydrogen. The photogenerated holes in the HOMO of PdTCPP⊂PCN-415(NH_2) were consumed by ascorbic acid.

g-C_3N_4 is characterized by its low cost, simple preparation, high nitrogen content, excellent stability and narrow band gap,

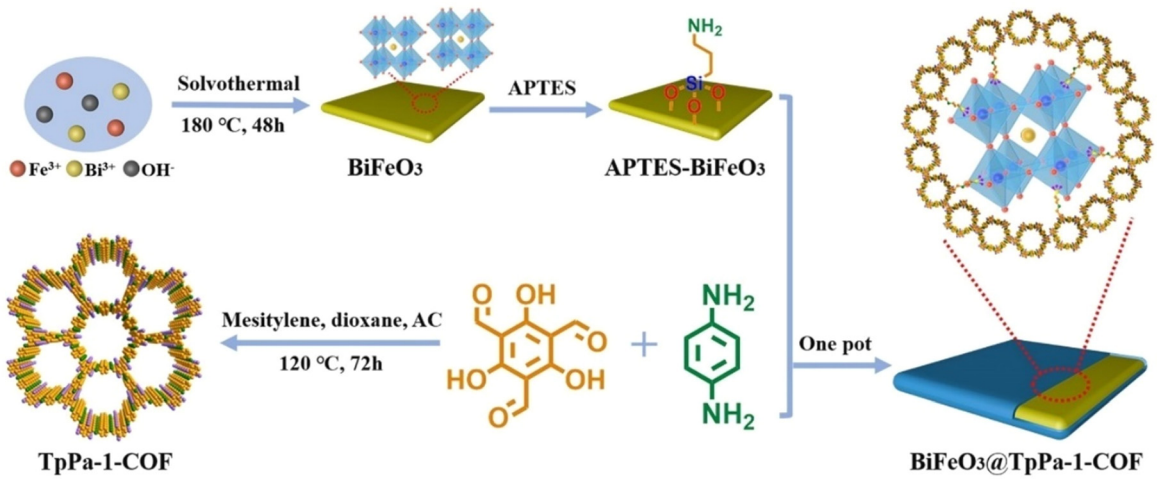

Fig. 18 Schematic illustration for fabricating a $BiFeO_3$@TpPa-1-COF core–shell Z-scheme heterojunction hybrid. Adapted with permission, copyright, 2022, Wiley-VCH.[123]

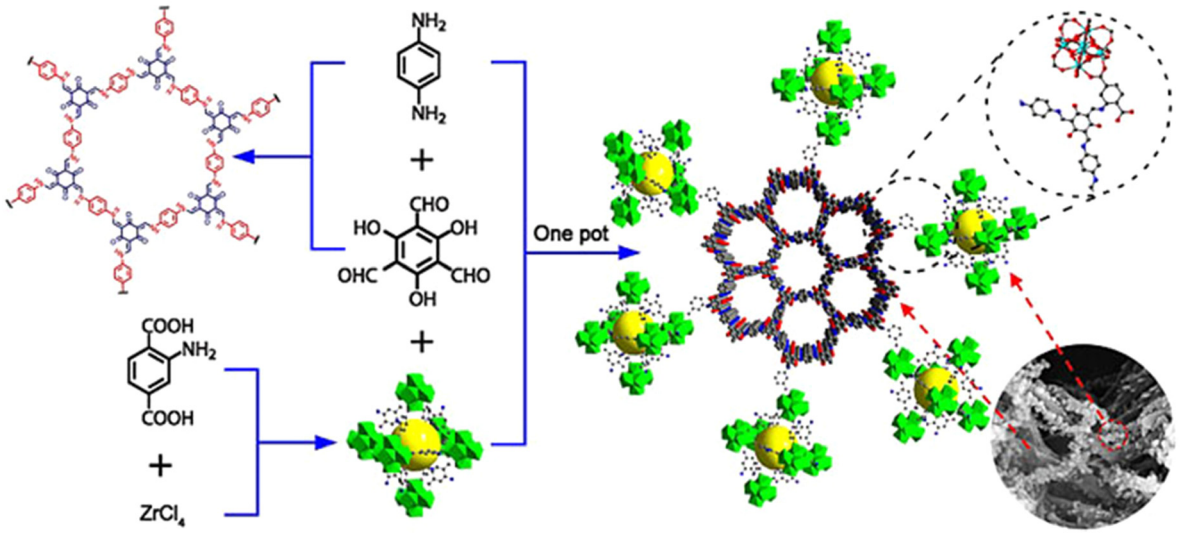

Fig. 19 Schematic illustration for designing an NH_2-UiO-66/TpPa-1-COF hybrid material. Adapted with permission, copyright, 2018, Wiley-VCH.[124]

making it useful for hybridization with COFs. Wang *et al.* reported a COF/g-C_3N_4 van der Waals heterojunction *via* an ultrasonic strategy.[141] With an increase in COF content, the COF/g-C_3N_4 heterojunction showed a significant red-shifting of the absorption band according to UV-vis diffuse reflectance spectroscopy, which demonstrated the enhanced photoresponse of the composite. The steady-state photoluminescence (PL) spectroscopy intensity of the COF/g-C_3N_4 heterojunction was lower than that of bare g-C_3N_4, further evidencing that the COF/g-C_3N_4 heterojunction exhibits a reduced electron–hole complexation rate. Excessive COF loading weakened the light absorption ability of g-C_3N_4 and reduced the number of catalytic active sites. When loading 12 wt% COF, the COF/g-C_3N_4 heterojunction indicated the best HER rate of 449.64 μmol h^{-1}, which was five-fold that of pure g-C_3N_4. Yan and co-workers modified g-C_3N_4 with a β-ketoenamine-linked COF as a hybrid material for H_2 photogeneration.[139] When 2 wt% Pt and triethanolamine were used as a co-catalyst and sacrificial agent, a H_2 performance of 10.1 mmol g^{-1} h^{-1} and AQE of 20.7% at 425 nm were attained.

5 Conclusions and outlook

In summary, compared with traditional inorganic semiconductors, COFs as a novel class of crystalline porous polymers have enormous potential for applications in the domain of photocatalysis due to their particular preponderances, and they can replace inorganic semiconductors to a certain extent. So far, in the domain of photocatalysis, COF materials have been applied in hydrogen generation, oxygen production, carbon dioxide reduction, organic reaction conversion and pollutant degradation. It is well known that COF-based photocatalytic hydrogen generation consists of three stages: light absorption, photoexcited charge carrier separation/transfer and surface redox reaction. In terms of whether these three processes can be performed, in this review, we mainly focused on linkage chemistry and proposing various strategies for boosting H_2 photoproduction performance.

Despite significant progress having been made in COF-based hydrogen photogeneration reactions, some matters still need to be urgently addressed. For instance, (1) most COFs display partially crystalline and they are polycrystals rather than single crystals, which somewhat reduces their photocatalytic activity. The discovery of single-crystal COFs is in the preliminary stages and a few synthetic methods have been discussed.[146–152] (2) Compared with the results achieved by 2D COFs in photocatalytic hydrogen precipitation, 3D COFs have been poorly explored. (3) Photocatalytic total hydrolysis for simultaneous hydrogen and oxygen evolution remains in its infancy. (4) More novel co-catalysts need to be prepared to replace expensive platinum. (5) The splendid activity of COF-based photocatalysts needs to be further exploited for the HER in the absence of Pt co-catalysts and sacrificial agents. (6) In addition to the HER rate, investigating the long-term stability of COF-based photocatalysts is also crucial. (7) Currently, the monomers for synthesizing COFs are relatively expensive and economically inefficient and remain in the laboratory research phase, making them arduous to manufacture in industrial production.

There is no denying the above drawbacks of COFs in this field. The following are some of the avenues that can be executed in the future. (1) Reasonable establishment of novel COFs with outstanding efficiency and stability is necessary. Chemistry and structure–function relationships can be understood more expressly from single crystals. The improvement of simpler and more general methods by which to synthesize stable single-crystal COFs is essential. The remarkable properties of triazine and bipyridine units in the field of COF-based photocatalytic hydrogen evolution have been testified in the available reports. Hence, establishing COF-based photocatalysts with a wider solar response range as well as strong electron delocalization is necessary. In addition, innovating novel linkages, especially olefin-linked COFs based on the Knoevenagel polycondensation

reaction, holds great potential. (2) Optimizing of synthesis routes. There are six strategies by which to construct COFs, including solvothermal,[153–155] microwave,[156–158] ionothermal,[159–161] room-temperature solution,[162–164] mechanochemical,[165–167] and interfacial methods.[168–170] The reaction temperature of ionothermal methods is too high and they are merely employed for establishing triazine-based COFs. Microwave methods require polar solvents to achieve better heating. Room-temperature solution, mechanochemical and interfacial methods are not appropriate to achieve a condensation reaction between the majority organic building blocks. Solvothermal methods are the most broadly employed means for constructing COFs. However, the rigorous conditions, such as a long reaction time and high temperature and pressure, restrict the use of such methods in commercial settings. Therefore, for COF-based photocatalytic hydrogen production, more efforts are imminently required to perform low-cost, short duration, simple reactions under mild conditions.

We believe this review will inspire interesting novel designs for the establishment of more efficient COF-based photocatalysts and that fundamental scientific knowledge will drive forward this new industry.

Conflicts of interest

There are no conflicts to declare.

Acknowledgements

This work was supported by the Hunan High-Level Talent Gathering Project-Innovation team (2021RC5030), the Construction of innovation demonstration zone of Chenzhou National Sustainable Development Agenda for innovative Hunan province (2021SFQ26), the Hunan Innovative Province Construction Special Funds project (2019SK2281) and the Environmental Protection Science and Technology Project of Hunan Province (Z202067380035). This work was also supported by the Hunan Key Technology R&D Program (2022GK2045) and the Changsha Municipal National Science Foundation (KQ2014120).

Notes and references

1 F. Sher, O. Curnick and M. T. Azizan, *Sustainability*, 2021, **13**, 2940.
2 K. H. Ng, S. Y. Lai, C. K. Cheng, Y. W. Cheng and C. C. Chong, *Chem. Eng. J.*, 2021, **417**, 128847.
3 H. Mikulčić, J. Baleta, J. J. Klemeš and X. Wang, *J. Cleaner Prod.*, 2021, **292**, 126027.
4 A. E. H. Berjawi, S. L. Walker, C. Patsios and S. H. R. Hosseini, *Renewable Sustainable Energy Rev.*, 2021, **145**, 111163.
5 L. Liu, S. Wang, H. Huang, Y. Zhang and T. Ma, *Nano Energy*, 2020, **75**, 104959.
6 D. Shindell and C. J. Smith, *Nature*, 2019, **573**, 408–411.
7 L. Schirone and F. Pellitteri, *Sustainability*, 2017, **9**, 2321.
8 Y. Chen, L. Feng, J. Wang and M. Höök, *Energy*, 2017, **128**, 540–549.
9 R. Fouquet, *Nat. Energy*, 2016, **1**, 16098.
10 T. Autrey and P. Chen, *J. Energy Chem.*, 2023, **77**, 119–121.
11 Z. Abdin, A. Zafaranloo, A. Rafiee, W. Mérida, W. Lipiński and K. R. Khalilpour, *Renewable Sustainable Energy Rev.*, 2020, **120**, 109620.
12 J. Ran, J. Qu, H. Zhang, T. Wen, H. Wang, S. Chen, L. Song, X. Zhang, L. Jing, R. Zheng and S.-Z. Qiao, *Adv. Energy Mater.*, 2019, **9**, 1803402.
13 J. Yan, *Nat. Clim. Change*, 2018, **8**, 560–561.
14 Y. Li, C.-K. Peng, H. Hu, S.-Y. Chen, J.-H. Choi, Y.-G. Lin and J.-M. Lee, *Nat. Commun.*, 2022, **13**, 1143.
15 Y.-J. Yuan, Z.-T. Yu, D.-Q. Chen and Z.-G. Zou, *Chem. Soc. Rev.*, 2017, **46**, 603–631.
16 D. Wang and X.-Q. Gong, *Nat. Commun.*, 2021, **12**, 158.
17 X. Lv, X. Li, C. Yang, X. Ding, Y. Zhang, Y.-Z. Zheng, S. Li, X. Sun and X. Tao, *Adv. Funct. Mater.*, 2020, **30**, 1910830.
18 D. Wang, Z.-P. Liu and W.-M. Yang, *ACS Catal.*, 2018, **8**, 7270–7278.
19 K. Chang, H. Pang, X. Hai, G. Zhao, H. Zhang, L. Shi, F. Ichihara and J. Ye, *Appl. Catal., B*, 2018, **232**, 446–453.
20 X. Hai, W. Zhou, K. Chang, H. Pang, H. Liu, L. Shi, F. Ichihara and J. Ye, *J. Mater. Chem. A*, 2017, **5**, 8591–8598.
21 Z.-F. Huang, J. Song, K. Li, M. Tahir, Y.-T. Wang, L. Pan, L. Wang, X. Zhang and J.-J. Zou, *J. Am. Chem. Soc.*, 2016, **138**, 1359–1365.
22 Z. Yu, Y. Li, A. Torres-Pinto, A. P. LaGrow, V. M. Diaconescu, L. Simonelli, M. J. Sampaio, O. Bondarchuk, I. Amorim, A. Araujo, A. M. T. Silva, C. G. Silva, J. L. Faria and L. Liu, *Appl. Catal., B*, 2022, **310**, 121318.
23 Y. Zhu, C. Lv, Z. Yin, J. Ren, X. Yang, C.-L. Dong, H. Liu, R. Cai, Y.-C. Huang, W. Theis, S. Shen and D. Yang, *Angew. Chem., Int. Ed.*, 2020, **59**, 868–873.
24 S. Yu, J. Li, Y. Zhang, M. Li, F. Dong, T. Zhang and H. Huang, *Nano Energy*, 2018, **50**, 383–392.
25 F. Lin, S. Zhou, G. Wang, J. Wang, T. Gao, Y. Su and C.-P. Wong, *Nano Energy*, 2022, **99**, 107432.
26 Q. Zhu, Z. Xu, B. Qiu, M. Xing and J. Zhang, *Small*, 2021, **17**, 2101070.
27 Z. Liang, Y. Xue, X. Wang, Y. Zhou, X. Zhang, H. Cui, G. Cheng and J. Tian, *Chem. Eng. J.*, 2021, **421**, 130016.
28 H. Hu, Z. Wang, L. Cao, L. Zeng, C. Zhang, W. Lin and C. Wang, *Nat. Chem.*, 2021, **13**, 358–366.
29 X. Feng, Y. Pi, Y. Song, C. Brzezinski, Z. Xu, Z. Li and W. Lin, *J. Am. Chem. Soc.*, 2020, **142**, 690–695.
30 B. Zhu, R. Zou and Q. Xu, *Adv. Energy Mater.*, 2018, **8**, 1801193.
31 X.-J. Kong, Z. Lin, Z.-M. Zhang, T. Zhang and W. Lin, *Angew. Chem., Int. Ed.*, 2016, **55**, 6411–6416.
32 D. Kim, D. R. Whang and S. Y. Park, *J. Am. Chem. Soc.*, 2016, **138**, 8698–8701.
33 D. Jiang, *Chem*, 2020, **6**, 2461–2483.
34 K. Geng, V. Arumugam, H. Xu, Y. Gao and D. Jiang, *Prog. Polym. Sci.*, 2020, **108**, 101288.
35 A. P. Côté, A. I. Benin, N. W. Ockwig, M. O'Keeffe, A. J. Matzger and O. M. Yaghi, *Science*, 2005, **310**, 1166–1170.
36 S. Karak, K. Dey and R. Banerjee, *Adv. Mater.*, 2022, **34**, 2202751.
37 Q. Guan, L.-L. Zhou and Y.-B. Dong, *Chem. Soc. Rev.*, 2022, **51**, 6307–6416.
38 R. Liu, K. T. Tan, Y. Gong, Y. Chen, Z. Li, S. Xie, T. He, Z. Lu, H. Yang and D. Jiang, *Chem. Soc. Rev.*, 2021, **50**, 120–242.
39 K. Geng, T. He, R. Liu, S. Dalapati, K. T. Tan, Z. Li, S. Tao, Y. Gong, Q. Jiang and D. Jiang, *Chem. Rev.*, 2020, **120**, 8814–8933.
40 M. S. Lohse and T. Bein, *Adv. Funct. Mater.*, 2018, **28**, 1705553.
41 S. Liu, M. Wang, Y. He, Q. Cheng, T. Qian and C. Yan, *Coord. Chem. Rev.*, 2023, **475**, 214882.
42 Y.-N. Gong, X. Guan and H.-L. Jiang, *Coord. Chem. Rev.*, 2023, **475**, 214889.
43 Y. Wang, Y. Zhao and Z. Li, *Macromol. Rapid Commun.*, 2022, **43**, 2200108.
44 S. Qiao, M. Di, J.-X. Jiang and B.-H. Han, *EnergyChem*, 2022, **4**, 100094.
45 X. Li, Q. Dong, Q. Tian, A. Sial, H. Wang, H. Wen, B. Pan, K. Zhang, J. Qin and C. Wang, *Mater. Today Chem.*, 2022, **26**, 101037.
46 J. You, Y. Zhao, L. Wang and W. Bao, *J. Cleaner Prod.*, 2021, **291**, 125822.
47 H. Wang, H. Wang, Z. Wang, L. Tang, G. Zeng, P. Xu, M. Chen, T. Xiong, C. Zhou, X. Li, D. Huang, Y. Zhu, Z. Wang and J. Tang, *Chem. Soc. Rev.*, 2020, **49**, 4135–4165.
48 S. Xu, M. Richter and X. Feng, *Acc. Mater. Res.*, 2021, **2**, 252–265.
49 T. He, K. Geng and D. Jiang, *Trends Chem.*, 2021, **3**, 431–444.
50 F. J. Uribe-Romo, C. J. Doonan, H. Furukawa, K. Oisaki and O. M. Yaghi, *J. Am. Chem. Soc.*, 2011, **133**, 11478–11481.

51 X. Zhuang, W. Zhao, F. Zhang, Y. Cao, F. Liu, S. Bi and X. Feng, *Polym. Chem.*, 2016, **7**, 4176–4181.
52 L. Stegbauer, K. Schwinghammer and B. V. Lotsch, *Chem. Sci.*, 2014, **5**, 2789–2793.
53 H. Yu, J. Zhang, X. Yan, C. Wu, X. Zhu, B. Li, T. Li, Q. Guo, J. Gao, M. Hu and J. Yang, *J. Mater. Chem. A*, 2022, **10**, 11010–11018.
54 W. Li, X. Huang, T. Zeng, Y. A. Liu, W. Hu, H. Yang, Y.-B. Zhang and K. Wen, *Angew. Chem., Int. Ed.*, 2021, **60**, 1869–1874.
55 Y. Wang, W. Hao, H. Liu, R. Chen, Q. Pan, Z. Li and Y. Zhao, *Nat. Commun.*, 2022, **13**, 100.
56 Z. Xie, X. Yang, P. Zhang, X. Ke, X. Yuan, L. Zhai, W. Wang, N. Qin, C.-X. Cui, L. Qu and X. Chen, *Chin. J. Catal.*, 2023, **47**, 171–180.
57 T. Zhou, X. Huang, Z. Mi, Y. Zhu, R. Wang, C. Wang and J. Guo, *Polym. Chem.*, 2021, **12**, 3250–3256.
58 Z. Zhao, Y. Zheng, C. Wang, S. Zhang, J. Song, Y. Li, S. Ma, P. Cheng, Z. Zhang and Y. Chen, *ACS Catal.*, 2021, **11**, 2098–2107.
59 Z. Zhao, X. Chen, B. Li, S. Zhao, L. Niu, Z. Zhang and Y. Chen, *Adv. Sci.*, 2022, **9**, 2203832.
60 J. Zhang, Y. Cao, W. Liu, T. Cao, J. Qian, J. Wang, X. Yao, A. Iqbal and W. Qin, *ChemSusChem*, 2022, **15**, e202101510.
61 J. Yang, J. Jing, W. Li and Y. Zhu, *Adv. Sci.*, 2022, **9**, 2201134.
62 Z. Xu, X. Cui, Y. Li, Y. Li, Z. Si and Q. Duan, *Appl. Surf. Sci.*, 2023, **613**, 155966.
63 G.-B. Wang, F.-C. Zhu, Q.-Q. Lin, J.-L. Kan, K.-H. Xie, S. Li, Y. Geng and Y.-B. Dong, *Chem. Commun.*, 2021, **57**, 4464–4467.
64 G.-B. Wang, H.-P. Xu, K.-H. Xie, J.-L. Kan, J. Fan, Y.-J. Wang, Y. Geng and Y.-B. Dong, *J. Mater. Chem. A*, 2023, **11**, 4007–4012.
65 G.-B. Wang, S. Li, C.-X. Yan, Q.-Q. Lin, F.-C. Zhu, Y. Geng and Y.-B. Dong, *Chem. Commun.*, 2020, **56**, 12612–12615.
66 C.-X. Liu, D.-L. Pan, Y. Seo, S. Park, J.-L. Kan, J. Y. Koo, W. Choi and E. Lee, *ACS Appl. Energy Mater.*, 2023, **6**, 1126–1133.
67 C. Lin, X. Liu, B. Yu, C. Han, L. Gong, C. Wang, Y. Gao, Y. Bian and J. Jiang, *ACS Appl. Mater. Interfaces*, 2021, **13**, 27041–27048.
68 W. Dong, Z. Qin, K. Wang, Y. Xiao, X. Liu, S. Ren and L. Li, *Angew. Chem., Int. Ed.*, 2023, **62**, e202216073.
69 C. Li, J. Liu, H. Li, K. Wu, J. Wang and Q. Yang, *Nat. Commun.*, 2022, **13**, 2357.
70 W. Chen, L. Wang, D. Mo, F. He, Z. Wen, X. Wu, H. Xu and L. Chen, *Angew. Chem., Int. Ed.*, 2020, **59**, 16902–16909.
71 V. S. Vyas, F. Haase, L. Stegbauer, G. Savasci, F. Podjaski, C. Ochsenfeld and B. V. Lotsch, *Nat. Commun.*, 2015, **6**, 8508.
72 L. Wang, L. Zhang, B. Lin, Y. Zheng, J. Chen, Y. Zheng, B. Gao, J. Long and Y. Chen, *Small*, 2021, **17**, 2101017.
73 J.-L. Sheng, H. Dong, X.-B. Meng, H.-L. Tang, Y.-H. Yao, D.-Q. Liu, L.-L. Bai, F.-M. Zhang, J.-Z. Wei and X.-J. Sun, *ChemCatChem*, 2019, **11**, 2313–2319.
74 L. Yin, Y. Zhao, Y. Xing, H. Tan, Z. Lang, W. Ho, Y. Wang and Y. Li, *Chem. Eng. J.*, 2021, **419**, 129984.
75 P. Xue, W. Chen, M. Tang, Z. Wang and Z. Wang, *Mol. Catal.*, 2023, **535**, 112807.
76 X. Wu, M. Zhang, Y. Xia, C. Ru, P. Chen, H. Zhao, L. Zhou, C. Gong, J. Wu and X. Pan, *J. Mater. Chem. A*, 2022, **10**, 17691–17698.
77 K. Wang, Z. Jia, Y. Bai, X. Wang, S. E. Hodgkiss, L. Chen, S. Y. Chong, X. Wang, H. Yang, Y. Xu, F. Feng, J. W. Ward and A. I. Cooper, *J. Am. Chem. Soc.*, 2020, **142**, 11131–11138.
78 K. Qian, X. Guan, N. Sun and H.-L. Jiang, *Sci. China: Chem.*, 2023, **66**, 436–442.
79 P. Pachfule, A. Acharjya, J. Roeser, T. Langenhahn, M. Schwarze, R. Schomäcker, A. Thomas and J. Schmidt, *J. Am. Chem. Soc.*, 2018, **140**, 1423–1427.
80 L. Hao, R. Shen, C. Huang, Z. Liang, N. Li, P. Zhang, X. Li, C. Qin and X. Li, *Appl. Catal., B*, 2023, **330**, 122581.
81 W. Li, X. Ding, B. Yu, H. Wang, Z. Gao, X. Wang, X. Liu, K. Wang and J. Jiang, *Adv. Funct. Mater.*, 2022, **32**, 2207394.
82 H. Liu, X. Zheng, J. Xu, X. Jia, M. Chao, D. Wang and Y. Zhao, *ACS Appl. Mater. Interfaces*, 2023, **15**, 16794.
83 E. Jin, Z. Lan, Q. Jiang, K. Geng, G. Li, X. Wang and D. Jiang, *Chem*, 2019, **5**, 1632–1647.
84 J.-P. Jeon, Y. J. Kim, S. H. Joo, H.-J. Noh, S. K. Kwak and J.-B. Baek, *Angew. Chem., Int. Ed.*, 2023, **62**, e202217416.
85 A. F. M. EL-Mahdy, A. M. Elewa, S.-W. Huang, H.-H. Chou and S.-W. Kuo, *Adv. Opt. Mater.*, 2020, **8**, 2000641.
86 S. Bi, C. Yang, W. Zhang, J. Xu, L. Liu, D. Wu, X. Wang, Y. Han, Q. Liang and F. Zhang, *Nat. Commun.*, 2019, **10**, 2467.
87 S. Bi, F. Meng, D. Wu and F. Zhang, *J. Am. Chem. Soc.*, 2022, **144**, 3653–3659.
88 S. Bi, C. Yang, W. Zhang, J. Xu, L. Liu, D. Wu, X. Wang, Y. Han, Q. Liang and F. Zhang, *Nat. Commun.*, 2019, **10**, 2467.
89 J. Wang, X.-X. Tian, L. Yu, D. J. Young, W.-B. Wang, H.-Y. Li and H.-X. Li, *J. Mater. Chem. A*, 2021, **9**, 25474–25479.
90 Z. Mi, T. Zhou, W. Weng, J. Unruangsri, K. Hu, W. Yang, C. Wang, K. A. I. Zhang and J. Guo, *Angew. Chem., Int. Ed.*, 2021, **60**, 9642–9649.
91 S. Yang, H. Lv, H. Zhong, D. Yuan, X. Wang and R. Wang, *Angew. Chem., Int. Ed.*, 2022, **61**, e202115655.
92 J. Yang, A. Acharjya, M.-Y. Ye, J. Rabeah, S. Li, Z. Kochovski, S. Youk, J. Roeser, J. Grüneberg, C. Penschke, M. Schwarze, T. Wang, Y. Lu, R. van de Krol, M. Oschatz, R. Schomäcker, P. Saalfrank and A. Thomas, *Angew. Chem., Int. Ed.*, 2021, **60**, 19797–19803.
93 H. Liu, Y. Li, L. Dai, X. Meng, A. Dong, Z. Zhou, H. Lv, P. Li and B. Wang, *Polym. Chem.*, 2023, **14**, 1323–1329.
94 S. Li, R. Ma, S. Xu, T. Zheng, G. Fu, Y. Wu, Z. Liao, Y. Kuang, Y. Hou, D. Wang, P. S. Petkov, K. Simeonova, X. Feng, L.-Z. Wu, X.-B. Li and T. Zhang, *J. Am. Chem. Soc.*, 2022, **144**, 13953–13960.
95 C. Mo, M. Yang, F. Sun, J. Jian, L. Zhong, Z. Fang, J. Feng and D. Yu, *Adv. Sci.*, 2020, **7**, 1902988.
96 Y. Yang, N. Luo, S. Lin, H. Yao and Y. Cai, *ACS Catal.*, 2022, **12**, 10718–10726.
97 R. Lu, C. Liu, Y. Chen, L. Tan, G. Yuan, P. Wang, C. Wang and H. Yan, *J. Photochem. Photobiol., A*, 2021, **421**, 113546.
98 Y. Chen, X. Luo, J. Zhang, L. Hu, T. Xu, W. Li, L. Chen, M. Shen, S.-B. Ren, D.-M. Han, G.-H. Ning and D. Li, *J. Mater. Chem. A*, 2022, **10**, 24620–24627.
99 L. Li, Y. Zhu, N. Gong, W. Zhang, W. Peng, Y. Li, F. Zhang and X. Fan, *Int. J. Hydrogen Energy*, 2020, **45**, 2689–2698.
100 S. Ma, T. Deng, Z. Li, Z. Zhang, J. Jia, Q. Li, G. Wu, H. Xia, S.-W. Yang and X. Liu, *Angew. Chem., Int. Ed.*, 2022, **61**, e202208919.
101 A. M. Elewa, A. F. M. El-Mahdy, A. E. Hassan, Z. Wen, J. Jayakumar, T.-L. Lee, L.-Y. Ting, I. M. A. Mekhemer, T.-F. Huang, M. H. Elsayed, C.-L. Chang, W.-C. Lin and H.-H. Chou, *J. Mater. Chem. A*, 2022, **10**, 12378–12390.
102 X. Wang, L. Chen, S. Y. Chong, M. A. Little, Y. Wu, W.-H. Zhu, R. Clowes, Y. Yan, M. A. Zwijnenburg, R. S. Sprick and A. I. Cooper, *Nat. Chem.*, 2018, **10**, 1180–1189.
103 W. Weng and J. Guo, *Nat. Commun.*, 2022, **13**, 5768.
104 W.-K. Han, Y. Liu, X. Yan, Y. Jiang, J. Zhang and Z.-G. Gu, *Angew. Chem., Int. Ed.*, 2022, **61**, e202208791.
105 R. Chen, Y. Wang, Y. Ma, A. Mal, X.-Y. Gao, L. Gao, L. Qiao, X.-B. Li, L.-Z. Wu and C. Wang, *Nat. Commun.*, 2021, **12**, 1354.
106 W. Zhou, Q.-W. Deng, H.-J. He, L. Yang, T.-Y. Liu, X. Wang, D.-Y. Zheng, Z.-B. Dai, L. Sun, C. Liu, H. Wu, Z. Li and W.-Q. Deng, *Angew. Chem., Int. Ed.*, 2023, **62**, e202214143.
107 Y. Zang, R. Wang, P.-P. Shao, X. Feng, S. Wang, S.-Q. Zang and T. C. W. Mak, *J. Mater. Chem. A*, 2020, **8**, 25094–25100.
108 J. Wang, L. Li, S. Jiang, D. J. Young, Z.-G. Ren and H.-X. Li, *ChemSusChem*, 2023, **16**, e202201943.
109 R. Shen, X. Li, C. Qin, P. Zhang and X. Li, *Adv. Energy Mater.*, 2023, **13**, 2203695.
110 X. Ren, C. Li, J. Liu, H. Li, L. Bing, S. Bai, G. Xue, Y. Shen and Q. Yang, *ACS Appl. Mater. Interfaces*, 2022, **14**, 6885–6893.
111 J. Ming, A. Liu, J. Zhao, P. Zhang, H. Huang, H. Lin, Z. Xu, X. Zhang, X. Wang, J. Hofkens, M. B. J. Roeffaers and J. Long, *Angew. Chem., Int. Ed.*, 2019, **58**, 18290–18294.
112 M. Lv, X. Ren, R. Cao, Z. Chang, X. Chang, F. Bai and Y. Li, *Polymers*, 2022, **14**, 4893.
113 Y. Li, L. Yang, H. He, L. Sun, H. Wang, X. Fang, Y. Zhao, D. Zheng, Y. Qi, Z. Li and W. Deng, *Nat. Commun.*, 2022, **13**, 1355.
114 J. Hu, H. Mehrabi, Y.-S. Meng, M. Taylor, J.-H. Zhan, Q. Yan, M. Benamara, R. H. Coridan and H. Beyzavi, *Chem. Sci.*, 2021, **12**, 7930–7936.
115 P. Dong, Y. Wang, A. Zhang, T. Cheng, X. Xi and J. Zhang, *ACS Catal.*, 2021, **11**, 13266–13279.
116 H. Dong, X.-B. Meng, X. Zhang, H.-L. Tang, J.-W. Liu, J.-H. Wang, J.-Z. Wei, F.-M. Zhang, L.-L. Bai and X.-J. Sun, *Chem. Eng. J.*, 2020, **379**, 122342.
117 B. P. Biswal, H. A. Vignolo-González, T. Banerjee, L. Grunenberg, G. Savasci, K. Gottschling, J. Nuss, C. Ochsenfeld and B. V. Lotsch, *J. Am. Chem. Soc.*, 2019, **141**, 11082–11092.

118 T. Banerjee, F. Haase, G. Savasci, K. Gottschling, C. Ochsenfeld and B. V. Lotsch, *J. Am. Chem. Soc.*, 2017, **139**, 16228–16234.
119 K. Gottschling, G. Savasci, H. Vignolo-González, S. Schmidt, P. Mauker, T. Banerjee, P. Rovó, C. Ochsenfeld and B. V. Lotsch, *J. Am. Chem. Soc.*, 2020, **142**, 12146–12156.
120 R. Gao, J. Bai, R. Shen, L. Hao, C. Huang, L. Wang, G. Liang, P. Zhang and X. Li, *J. Mater. Sci. Technol.*, 2023, **137**, 223–231.
121 M.-Y. Gao, C.-C. Li, H.-L. Tang, X.-J. Sun, H. Dong and F.-M. Zhang, *J. Mater. Chem. A*, 2019, **7**, 20193–20200.
122 Y.-P. Zhang, W. Han, Y. Yang, H.-Y. Zhang, Y. Wang, L. Wang, X.-J. Sun and F.-M. Zhang, *Chem. Eng. J.*, 2022, **446**, 137213.
123 M.-L. Xu, M. Lu, G.-Y. Qin, X.-M. Wu, T. Yu, L.-N. Zhang, K. Li, X. Cheng and Y.-Q. Lan, *Angew. Chem., Int. Ed.*, 2022, **61**, e202210700.
124 F.-M. Zhang, J.-L. Sheng, Z.-D. Yang, X.-J. Sun, H.-L. Tang, M. Lu, H. Dong, F.-C. Shen, J. Liu and Y.-Q. Lan, *Angew. Chem., Int. Ed.*, 2018, **57**, 12106–12110.
125 C.-X. Chen, Y.-Y. Xiong, X. Zhong, P. C. Lan, Z.-W. Wei, H. Pan, P.-Y. Su, Y. Song, Y.-F. Chen, A. Nafady Sirajuddin and S. Ma, *Angew. Chem., Int. Ed.*, 2022, **61**, e202114071.
126 H.-Y. Zhang, Y. Yang, C.-C. Li, H.-L. Tang, F.-M. Zhang, G.-L. Zhang and H. Yan, *J. Mater. Chem. A*, 2021, **9**, 16743–16750.
127 P. Xue, X. Pan, J. Huang, Y. Gao, W. Guo, J. Li, M. Tang and Z. Wang, *ACS Appl. Mater. Interfaces*, 2021, **13**, 59915–59924.
128 L.-H. Shao, A.-X. Huang, X.-C. Yan, Y.-H. Liu, Y. Wang, X. Jin and F.-M. Zhang, *J. Colloid Interface Sci.*, 2023, **633**, 233–242.
129 T. Zhou, L. Wang, X. Huang, J. Unruangsri, H. Zhang, R. Wang, Q. Song, Q. Yang, W. Li, C. Wang, K. Takahashi, H. Xu and J. Guo, *Nat. Commun.*, 2021, **12**, 3934.
130 Y.-P. Zhang, H.-L. Tang, H. Dong, M.-Y. Gao, C.-C. Li, X.-J. Sun, J.-Z. Wei, Y. Qu, Z.-J. Li and F.-M. Zhang, *J. Mater. Chem. A*, 2020, **8**, 4334–4340.
131 Y. Zhang, Y. Li, J. Yu, B. Sun and H. Shang, *Molecules*, 2023, **28**, 822.
132 M. Yan, F. Jiang and Y. Wu, *Int. J. Hydrogen Energy*, 2023, **48**, 8867–8876.
133 H. Yan, Y.-H. Liu, Y. Yang, H.-Y. Zhang, X.-R. Liu, J.-Z. Wei, L.-L. Bai, Y. Wang and F.-M. Zhang, *Chem. Eng. J.*, 2022, **431**, 133404.
134 G. Yan, X. Sun, K. Zhang, Y. Zhang, H. Li, Y. Dou, D. Yuan, H. Huang, B. Jia, H. Li and T. Ma, *Small*, 2022, **18**, 2201340.
135 H. Wang, C. Qian, J. Liu, Y. Zeng, D. Wang, W. Zhou, L. Gu, H. Wu, G. Liu and Y. Zhao, *J. Am. Chem. Soc.*, 2020, **142**, 4862–4871.
136 J. Tang, Q. Li, Y. Liu, N. Xu, K. Wang, Q. Zhang, W. Yang and Y. Fan, *Int. J. Hydrogen Energy*, 2021, **46**, 17666–17676.
137 L. Sun, W. Wang, T. Kong, H. Jiang, H. Tang and Q. Liu, *J. Mater. Chem. A*, 2022, **10**, 22531–22539.
138 D. Shang, D. Li, B. Chen, B. Luo, Y. Huang and W. Shi, *ACS Sustainable Chem. Eng.*, 2021, **9**, 14238–14248.
139 M. Luo, Q. Yang, K. Liu, H. Cao and H. Yan, *Chem. Commun.*, 2019, **55**, 5829–5832.
140 Y. Liu, H. Tan, Y. Wei, M. Liu, J. Hong, W. Gao, S. Zhao, S. Zhang and S. Guo, *ACS Nano*, 2023, **17**, 5994–6001.
141 Y. Liu, L. Jiang, Y. Tian, Z. Xu, W. Wang, M. Qiu, H. Wang, X. Li, G. Zhu and Y. Wang, *Inorg. Chem.*, 2023, **62**, 3271–3277.
142 Z. Liang, R. Shen, P. Zhang, Y. Li, N. Li and X. Li, *Chin. J. Catal.*, 2022, **43**, 2581–2591.
143 T. He, W. Zhen, Y. Chen, Y. Guo, Z. Li, N. Huang, Z. Li, R. Liu, Y. Liu, X. Lian, C. Xue, T. C. Sum, W. Chen and D. Jiang, *Nat. Commun.*, 2023, **14**, 329.
144 P. Dong, T. Cheng, J.-L. Zhang, J. Jiang, L. Zhang, X. Xi and J. Zhang, *ACS Appl. Energy Mater.*, 2023, **6**, 1103–1115.
145 Y.-J. Cheng, R. Wang, S. Wang, X.-J. Xi, L.-F. Ma and S.-Q. Zang, *Chem. Commun.*, 2018, **54**, 13563–13566.
146 T. Liu, Y. Zhao, M. Song, X. Pang, X. Shi, J. Jia, L. Chi and G. Lu, *J. Am. Chem. Soc.*, 2023, **145**, 2544–2552.
147 A. Natraj, W. Ji, J. Xin, I. Castano, D. W. Burke, A. M. Evans, M. J. Strauss, M. Ateia, L. S. Hamachi, N. C. Gianneschi, Z. A. Alothman, J. Sun, K. Yusuf and W. R. Dichtel, *J. Am. Chem. Soc.*, 2022, **144**, 19813–19824.
148 C. Kang, K. Yang, Z. Zhang, A. K. Usadi, D. C. Calabro, L. S. Baugh, Y. Wang, J. Jiang, X. Zou, Z. Huang and D. Zhao, *Nat. Commun.*, 2022, **13**, 1370.
149 L. Liang, Y. Qiu, W. D. Wang, J. Han, Y. Luo, W. Yu, G.-L. Yin, Z.-P. Wang, L. Zhang, J. Ni, J. Niu, J. Sun, T. Ma and W. Wang, *Angew. Chem., Int. Ed.*, 2020, **59**, 17991–17995.
150 J. A. R. Navarro, *Science*, 2018, **361**, 35.
151 T. Ma, E. A. Kapustin, S. X. Yin, L. Liang, Z. Zhou, J. Niu, L.-H. Li, Y. Wang, J. Su, J. Li, X. Wang, W. D. Wang, W. Wang, J. Sun and O. M. Yaghi, *Science*, 2018, **361**, 48–52.
152 A. M. Evans, L. R. Parent, N. C. Flanders, R. P. Bisbey, E. Vitaku, M. S. Kirschner, R. D. Schaller, L. X. Chen, N. C. Gianneschi and W. R. Dichtel, *Science*, 2018, **361**, 52–57.
153 Q. Zhang, S. Dong, P. Shao, Y. Zhu, Z. Mu, D. Sheng, T. Zhang, X. Jiang, R. Shao, Z. Ren, J. Xie, X. Feng and B. Wang, *Science*, 2022, **378**, 181–186.
154 Z. Shan, M. Wu, D. Zhu, X. Wu, K. Zhang, R. Verduzco and G. Zhang, *J. Am. Chem. Soc.*, 2022, **144**, 5728–5733.
155 Y. Liu, Y. Ma, Y. Zhao, X. Sun, F. Gándara, H. Furukawa, Z. Liu, H. Zhu, C. Zhu, K. Suenaga, P. Oleynikov, A. S. Alshammari, X. Zhang, O. Terasaki and O. M. Yaghi, *Science*, 2016, **351**, 365–369.
156 L. K. Beagle, D. C. Moore, G. Kim, L. D. Tran, P. Miesle, C. Nguyen, Q. Fang, K.-H. Kim, T. A. Prusnik, M. Newburger, R. Rao, J. Lou, D. Jariwala, L. A. Baldwin and N. R. Glavin, *ACS Appl. Mater. Interfaces*, 2022, **14**, 46876–46883.
157 B. Díaz de Greñu, J. Torres, J. García-González, S. Muñoz-Pina, R. de los Reyes, A. M. Costero, P. Amorós and J. V. Ros-Lis, *ChemSusChem*, 2021, **14**, 208–233.
158 H. Wei, S. Chai, N. Hu, Z. Yang, L. Wei and L. Wang, *Chem. Commun.*, 2015, **51**, 12178–12181.
159 X. Yang, L. Gong, K. Wang, S. Ma, W. Liu, B. Li, N. Li, H. Pan, X. Chen, H. Wang, J. Liu and J. Jiang, *Adv. Mater.*, 2022, **34**, 2207245.
160 H. Wei, J. Ning, X. Cao, X. Li and L. Hao, *J. Am. Chem. Soc.*, 2018, **140**, 11618–11622.
161 J. Maschita, T. Banerjee, G. Savasci, F. Haase, C. Ochsenfeld and B. V. Lotsch, *Angew. Chem., Int. Ed.*, 2020, **59**, 15750–15758.
162 J. He, B. Luo, H. Zhang, Z. Li, N. Zhu, F. Lan and Y. Wu, *J. Colloid Interface Sci.*, 2022, **606**, 1333–1339.
163 G. Lin, C. Gao, Q. Zheng, Z. Lei, H. Geng, Z. Lin, H. Yang and Z. Cai, *Chem. Commun.*, 2017, **53**, 3649–3652.
164 Y. Peng, W. K. Wong, Z. Hu, Y. Cheng, D. Yuan, S. A. Khan and D. Zhao, *Chem. Mater.*, 2016, **28**, 5095–5101.
165 S. T. Emmerling, L. S. Germann, P. A. Julien, I. Moudrakovski, M. Etter, T. Friščić, R. E. Dinnebier and B. V. Lotsch, *Chem*, 2021, **7**, 1639–1652.
166 D. B. Shinde, H. B. Aiyappa, M. Bhadra, B. P. Biswal, P. Wadge, S. Kandambeth, B. Garai, T. Kundu, S. Kurungot and R. Banerjee, *J. Mater. Chem. A*, 2016, **4**, 2682–2690.
167 B. P. Biswal, S. Chandra, S. Kandambeth, B. Lukose, T. Heine and R. Banerjee, *J. Am. Chem. Soc.*, 2013, **135**, 5328–5331.
168 H. Wang, J. Zhao, Y. Li, Y. Cao, Z. Zhu, M. Wang, R. Zhang, F. Pan and Z. Jiang, *Nano-Micro Lett.*, 2022, **14**, 216.
169 D. Yadav, A. Kumar, J. Y. Kim, N.-J. Park and J.-O. Baeg, *J. Mater. Chem. A*, 2021, **9**, 9573–9580.
170 R. Wang, X. Shi, A. Xiao, W. Zhou and Y. Wang, *J. Membr. Sci.*, 2018, **566**, 197–204.